Identifying the Effect of Vibration on Crack Growth in Shaft Using Fuzzy Logic Algorithm

Jimma University

Jimma institute of Technology

Graduate School of Mechanical Engineering

By

Getasew Andargie Ademe

Thesis submitted to the School of Graduate Studies of
Jimma University in partial fulfilment of the Requirements
for the Degree of Master of Science in Mechanical Engineering
(Design of Mechanical System)

Jimma, Ethiopia

January 2022 G.C

Identifying the Effect of Vibration on Crack Growth in Shaft Using Fuzzy Logic Algorithm

By

Getasew Andargie Ademe

Main Advisor: Dr-Ing. Mesay Alemu (Ph.D., Assoc. Prof.)

Co-Advisor: Mr. Yohanis Dabesa (MSc.)

Thesis submitted to the School of Graduate Studies of Jimma University in partial fulfilment of the Requirements for the Degree of Master of Science in Mechanical Engineering (Design of Mechanical System)

Jimma, Ethiopia

January 2022 G.C

Declaration

By my signature below, I declare and affirm that this thesis is my work. I have followed all ethical and technical principles in the literature review, mathematical modelling, Ansys-based modal analysis, and the fuzzy logic method of crack identification.

Declared by:

Getasew Andargie Ademe	_____	_____
Name	Signature	Date

As a University advisor, I have approved the submission of this thesis for examination.

Confirmed by advisors:

Name	**Signature**	**Date**
Dr-Ing. Mesay Alemu (Ph.D., Assoc. Prof.)	_____	_____
(**Main Advisor**)		
Mr. Yohanis Dabesa (MSc.)	_____	_____
(**Co-Advisor**)		

Jimma University

Jimma institute of Technology

School of Graduate Studies

Faculty of Mechanical Engineering

Approval Sheet

As a member of the examining board of open defense, we have checked and evaluated the Master's Thesis prepared and presented by Getasew Andargie Ademe entitled **'Identifying the Effect of Vibration on Crack Growth in Shaft Using Fuzzy Logic Algorithm'**. Hereby we certify this work fulfilled the requirement of the Degree of Master of Science in Mechanical Engineering (Design of Mechanical System).

Examination Committees

Name	**Signature**	**Date**
Dr-Ing. Mesay Alemu (Ph.D., Assoc. Prof.)		
(**Main Advisor**)		
Mr. Yohanis Dabesa (MSc.)		
(**Co-Advisor**)		
Dr-Ing. Getachew Shunki (Ph.D., Assoc. Prof.)		
(**External Examiner**)		
Dr-Eng. Johnson Santhosh (Ph.D.)		
(**Internal Examiner**)		
Mr. Fakada Dabalo (MSc.)		
(**Chairman**)		

Acknowledgments

First I would like to thank the almighty God, for giving me this opportunity. Next, I would like to express my gratitude to Dr-Ing. Mesay Alemu (Ph.D., Assoc. Prof.) for his comment, direction, and support in this work. His passion and rigorous attitude towards research is always an inspiration for me. Without his continuous support and guidance, as well as his encouragement during difficult periods, the completion of this thesis work would not possible.

Along with Dr-Ing. Mesay, I would like to thank Mr. Yohanis Dabesa (Ph.D. student at Silesian University of Technology, Poland), my co-advisor for his comment and careful suggestions with regards to this work. Also, I would like to thank Mr. Iyasu Tafese (MSc., Program coordinator of Systems of Mechanical Design Stream) for his moral support and valuable suggestions.

I would like to thank all the members of the Faculty of Mechanical Engineering, and the Institute who helped me in various ways towards the completion of my work. I am also very grateful to my friend Mr. Daniel Dessalegn (Maintenance and Operation Engineer at Ethiopian Electric Power) who supported me in my everyday questions and problems related to work on this thesis.

Last but not the least, a special word of gratitude and appreciation goes to my family for their sincere support and constant encouragement during my study.

Abstract

Cracks in shafts can be identified as a significant factor for limiting the safe and reliable operation of machines. Engineers can predict faults using classical approaches. However, when artificial intelligence approaches are used, the forecasting time for crack diagnosis improves dramatically. The objective of this study is to detect the location and depth of the crack in the shaft using a fuzzy logic algorithm. Literature presents measurements of frequency, mode shape, and structural damping can be used to assess cracks. However, evaluating mode shape and structural deformation is more difficult than measuring frequency. Such criteria, however, are insufficiently sensitive to detect early flaws. This study employs changes in phase angle and natural frequency as crack indicators. To evaluate the natural frequencies and phase angles of the cracked shaft utilizing the change in stiffness matrices of the cracked element, theoretical calculations were performed using Matlab. To verify the theoretical values of natural frequencies, modal analysis was performed using Ansys. Good agreement is observed between the results. To detect the location and depth of the crack, the fuzzy logic technique uses first and second mode natural frequencies and their corresponding phase angles of the shaft as input parameters. The correlation coefficients for triangular, trapezoidal, and Gaussian membership functions are all close to one. Also, the average total errors of the three membership functions with the theoretical values are all less than 5%. This indicates that results obtained from all membership functions are close to the theoretical locations and depths of crack. So the proposed fuzzy logic technique would constitute an efficient tool for real-time crack identification.

keywords: Crack identification, Natural frequency, Phase angle, Mode shape, Fuzzy logic, Finite Element Analysis

List of Abbreviations

AI	Artificial Intelligence
ANN	Artificial Neural Network
$BPNN$	Back-Propagation Neural Network
$BSWI$	B-Spline Wavelet on the Interval
CNN	Convolutional Neural Network
EMA	Experimental Modal Analysis
FE	Finite Element
FEA	Finite Element Analysis
FEM	Finite Element Method
FL	Fuzzy Logic
GA	Genetic Algorithm
LDV	Laser Doppler Vibrometer
MCS	Monte Carlo simulation
PSD	Power Spectral Density
$PSVM$	Proximal Support Vector Machines
PZT	Piezoelectric Patch
$SIMO$	Single-Input Multi-Output
LDV	Laser Doppler Vibrometer
VMD	Variation Mode Decomposition
VMT	Vibration Monitoring Techniques

Symbols

u	Displacement in x-axis direction relative to the fixed reference in space
v	Displacement in y-axis direction relative to the fixed reference in space
θ	Rotation about x-axis relative to the fixed reference in space
ψ	Rotation about y-axis relative to the fixed reference in space
T_d	Total Kinetic Energy of disc
$\dot{u}$	Linear velocities in x direction
$\dot{v}$	Linear velocities in y direction
$\dot{\check{\theta}}$	Instantaneous angular velocities about the $\check{x}$- axis
$\dot{\check{\psi}}$	Instantaneous angular velocities about the $\check{y}$- axis
$\dot{\check{\emptyset}}$	Instantaneous angular velocities about the $\check{z}$ axis
M_d	Mass of the disc
$[T]$	Transformation matrix
{q}	Displacement vector
m_d^e	Element mass matrix
G_d^e	Element gyroscopic matrix
$u_e(\xi, t)$	Lateral displacement of the beam neutral plane
E_e	Element Young‘s modulus
ξ	Local element displacement
$N_{ei}(\xi)$	Shape functions
I_e	Second moment of area of the cross section about the neutral axis
U_e	Element strain energy
N_{ei}''	Second derivatives of the shape function
T_e	Kinetic energy
ρ_e	Mass density
A_e	Beam cross-section area

ψ_e	Beam cross-section angle
I_p	Polar moment of inertia
I_d	Transverse moment of inertia
k_{uu}	Bearing horizontal stiffness
k_{vv}	Bearing vertical stiffness
k_{uv}	Bearing cross stiffness
K_b	Stiffness matrix of the bearings
C_b	Damping matrix of bearings
c_{uu}	Bearing horizontal damping
c_{vv}	Bearing vertical damping
c_{vu}	Bearing cross damping
$\mathbf{q}(t)$	Nodal displacement vector
$\mathbf{M}$	Global mass matrix
$\mathbf{C}$	Global damping matrix
$\mathbf{K}$	Global stiffness matrix
$\mathbf{G}$	Global gyroscopic matrix
ϕ	Crack angle
ϕ_p	Phase angle
Ω	Rotor speed
$I_{\tilde{x}}$	Second moment of area centroidal $\check{X}$
$I_{\tilde{y}}$	Second moment of area centroidal $\check{Y}$
l_{ce}	Cracked element length
$I_{\tilde{x}}(t)$	Time-varying second moment of area of the cracked element about $\check{X}$
$I_{\tilde{y}}(t)$	Time-varying second moment of area of the cracked element about $\check{Y}$
A_1	Un-cracked area left
e	Y-axis centroidal location
R	Radius of the shaft
A_{ce}	Overall cross-sectional area of the cracked element
μ	Crack depth ratio
I_x	Second moment of area of cracked cross-sections in horizontal direction
I_y	Second moment of area of cracked cross-sections in vertical direction
I	Second moment of area of Un-cracked shaft

Table of Contents

List of Figures

List of Tables

Chapter 1

Introduction

1.1 Background

For several decades, diagnosing cracks in rotating machinery has been a research problem for industries. Such cracks can result in complete failure of the system, resulting in significant downtime expenses. As a result, owners of important plant machinery are especially interested in the early detection of symptoms that can lead to machinery and equipment breakdown in the field [1].

Condition monitoring techniques are required for the safe and cost-effective operation of rotor dynamic machinery. Because these techniques evaluate the health of machinery on a regular or continuous basis to ensure that it continues to function properly [2, 3]. Condition monitoring in rotor dynamic systems is classified as either off-line or on-line [4]. When the shaft has stopped rotating, offline condition monitoring is undertaken. Visual examination, ultrasound procedures, static deflection testing, and other off-line condition monitoring methods are all available. These off-line condition monitoring approaches necessitate periodic inspection and repair, resulting in costly downtime.

On-line condition monitoring is carried out while the machine is in normal operation, avoiding costly and time-consuming downtime [5]. On-line condition monitoring for rotating machinery provides various advantages to the operator.

i. Rather than relying on regular periodic maintenance, repairs can be made as needed. For large turbomachinery systems, such as power-generating steam tur-

bines, the cost of periodic maintenance is frequently prohibitive.

ii. Online condition monitoring can give you a real-time diagnosis of the severity of an issue. The operator can decide whether to continue operating the equipment or fix it based on the severity of the malfunction.

iii. By giving a continuous evaluation of fault propagation, online condition monitoring reduces the risk of abrupt failure.

In different engineering systems (steel structures, industrial machinery, aerospace industry) rotary machines have several applications, such as engines and electrical generators, hydraulic turbines, pumps, compressors, wellbore construction, and others. Due to the loading, normal operations, accidents, and environmental effects they may experience cracks, which drastically reduce the life cycle of the structural system [6].

In a typical facility, a variety of predictive maintenance approaches are employed to monitor and analyze essential rotating machines and equipment. Visual inspection, thermography, vibration analysis, tribology, process monitoring, ultrasonic, and others are examples of non-destructive analysis techniques [7]. Because vibration analysis is non-destructive and does not interfere with the machine's normal operation, it is the most popular predictive maintenance technique utilized with maintenance management applications. Early crack detection plays an important role in the evaluation of rotary machines that are driven by rotating shafts which constitute the main component (or heart) of these high-performance rotating systems to ensure their safety.

Although shafts are carefully designed for fatigue loading and a high level of safety by using high-quality materials and precise manufacturing techniques, disastrous failures of rotors as a consequence of cracks still exist [6]. This is especially true in high-speed rotating machinery where the shaft carries discs, blades, gears, and other components, which are sources of generating mechanical stresses such as flexural, torsional, axial radial, and shear forces during shaft rotation. As a result, the local stresses due to fatigue cracks will increase and become more than the yield strength of the shaft material. Therefore, it is important to constantly monitor the technical condition of a given rotating machine and quickly react to possible changes resulting from developing failures.

Over time, the depth of the crack propagates until it reaches a limiting value beyond which the shaft cannot withstand the static and dynamic load anymore and a sudden fracture of the shaft occurs. According to their orientation concerning the shaft axis, there are three types of cracks. These are transverse cracks, longitudinal cracks, and slant cracks. Transverse cracks are the most serious and most common defects in rotating systems. They are perpendicular to the axis of a shaft. They reduce the cross-sectional area of the shaft and produce serious damages to the shaft [8]. Cracks parallel to the shaft's axis are known as longitudinal cracks. They are relatively uncommon and less serious. Slant cracks are cracks that appear at an angle to the axis of the shaft and they occur less frequently compared to transverse cracks. This thesis aims to determine the crack signature parameters and identify the location and depth of crack in shaft using intelligent technique.

1.2 Statement of the Problem

Cracks in a shaft arise in different configurations and severity can be developed during the operation of rotating machines. If a crack propagates continuously and is not detected, abrupt failure may occur and finally lead to the plant shutdown with associated various losses (enormous costs in downtime, equipment damage, and the risk of worker injury). Hence, the presence of cracks should be identified well before it goes critical and leads to an abrupt failure. Using classical methods, engineers can predict faults. The visual inspection approach is the most commonly used way for collecting crack details such as presence, position, and width, which can be used for maintenance. Even though it is the most generally used method, it has several disadvantages, including being costly, time-consuming, labor-intensive, and sometimes inaccurate due to a lack of knowledge. So, there is a need for a very efficient and precise tool for identifying crack locations that are extremely close to exact. Artificial intelligence techniques, as opposed to other ways, are gaining a lot of traction in this respect due to their ease of use, reliability, accuracy, and precision.

1.3 Objectives of the Study

1.3.1 General objective

The general objective of this study is to detect the location and depth of crack in the rotating shaft using the Fuzzy Logic (FL) technique.

1.3.2 Specific objectives

- To model the uncracked and cracked shaft theoretically. In all these theoretical approaches transverse crack has been analyzed.
- To develop three-dimensional models of the shaft using Solidwork premium.
- To obtain modal natural frequencies and corresponding mode shapes using Matlab and Ansys workbenches.
- To determine fuzzy sets and membership functions.
- The data obtained from the theoretical analysis have been trained to the fuzzy controller for designing the rule base for the detection of crack depth and crack location.

1.4 Motivation

Because of the frequent disaster of such rotors in engineering applications, vibration analysis of the rotor has been given high importance in the field of vibration. To avoid sudden and unexpected failure of the rotor systems, the development of health monitoring tools is critical. Shafts with cracks, defects, or damage pose a major threat to the system's current and future performance. The presence of faults on structures and rotating machine elements in case of cyclic loading may cause severe abrupt failure and finally lead to the plant shutdown with associated various losses. So, to overcome these losses and sustain structural stability, early diagnosing and localization of defects is required. Researchers, engineers, and scientists have produced a variety of procedures, analyses, and experiments that provide aspiration and support for new re-

search. The existence of cracks in structures degrades their behaviour to a certain extent.

Various scholars have devised several ways for identifying structural faults. The majority of technologies (magnetic particle testing, gamma radiation, X-ray testing, ultrasonic testing, and so on) are confined to local damage detection, are less sensitive, and are therefore more expensive. Vibration-based damage detection techniques, on the other hand, are global in scope and extremely sensitive. One of the requirements for fault diagnosis of structures is a change in dynamic behavior caused by a crack. Thus an effort has been given to formulate some intelligent techniques for localization and identification of cracks in rotor shafts, which is the FL algorithm.

1.5 Significance of the Study

The cracks are the main source of hazardous failure both in static and dynamic conditions. As a result, early detection of a rotor crack could help to prevent serious damage and costly repairs caused by rotating machinery failure, as well as ensure worker safety. Thus it is very crucial to develop an online crack detection mechanism, like Artificial Intelligence (AI) techniques by considering essential parameters. Because these techniques are non-destructive.

1.6 Scope of the Study

The scope of this thesis is constructed to establish a new methodology that predicts the crack location and the crack depth of the shaft with considerably less computational time and high precision. This study includes the theoretical and FE modelling of both the cracked and the uncracked shafts, determining the responses of crack signature parameters using Matlab and Ansys simulation environments, and training the crack signature parameters for identification of crack (knowing the location and depth of crack) using FL technique.

1.7 Contribution of the Thesis

The contributions that have been achieved in this study are listed below.

i. It is known that changes in a shaft's natural frequencies caused by the presence of a crack are quite minor. As a result, crack identification should not rely solely on changes in natural frequency. This study, however, presents a method for overcoming this challenge that employs changes in phase angle and natural frequency as crack indicators. To identify and locate a crack, the method analyzes crack signatures such as changes in natural frequency and phase angle.

ii. The idea of change in natural frequency and change in phase angle has been implemented theoretically on turbine rotating shafts. The numerical simulations from Ansys show that the dynamics of cracked shafts have an impact on change in natural frequency. The numerical simulations from Matlab show that the dynamics of cracked shafts have a significant impact on change in phase angle and change in natural frequency and all this enables the developed approach for identification of cracks in shafts.

iii. The FL method using three different membership functions was developed for the location and identification of cracks in rotating turbine shafts.

1.8 Organization of the Thesis

The entire research work is organized into seven chapters.

The theoretical background, statement of the problem, general and specific objectives, motivation of the study, and scope of the study are clearly defined in chapter one. Following Chapter one, the previous works related to this study, the historical outlooks of crack identification methods, and their comparative advantage are reviewed in Chapter two. In Chapter Three, the background of basic theoretical principles and mathematical model of the uncracked and cracked turbine shaft is defined. Chapter four deals with the Ansys based modal analysis of both cracked and intact shafts.

In Chapter Five, the identification of the crack location and crack depth using the FL algorithm is defined. Chapter six deals with results and discussion obtained from the forward and backward methods. The forward methods are theoretical methods (using Matlab and Ansys) used to determine the crack signature parameters, and backward methods are methods used to identify the location and depth of crack using crack signature parameters. Also, the application of the fuzzy logic technique is defined in this chapter. Lastly, Chapter seven deals with general conclusions as well as recommendations for further research. Reference and Appendix are mentioned at the end of the document.

Chapter 2

Literature Review

2.1 Introduction

Currently, crack detection is one of the most important areas of research. Many scholars have conducted considerable researches throughout the years to create structural integrity monitoring tools to avert failure caused by cracks. Most of the researchers are doing their research work related to crack detection using various techniques.

2.2 Analysis of Different Methodologies for Crack Identification in Shaft

2.2.1 Vibration based methods for crack identification

The vibration-based method is included prominently in the published literature on crack diagnosis and identification. These techniques can be further sub-classified into signal-based and model-based approaches. Signal-based approaches use typical vibration monitoring equipment (such as proximity probes, phase reference, and spectrum analyzers) with or without extra systems (such as torsional vibration measurement) [9, 10]. Model-based methods simulate the behavior of cracked shafts during operation by using analytical or numerical models. These methods attempt to correlate the vibration signature with the occurrence of a crack at certain points on the shaft [11–13].

To create a damage detection method, Cerri et al. [14] offered a theoretical study for the vibration-based examination of a circular arch in both faulty and non-faulty models.

For validation, they compared the theoretical analysis results with the results of the experimental analysis. They developed a damage detection model based on mode shapes and natural frequencies, assuming that the arch acts as a torsion spring on the fractured part. Wang et al. [12] investigated the vibration and stability analysis of a bearing-rotor system with transverse breathing crack and initial bending. They showed how early bending causes changes in breathing functions for the transverse breathing crack, and how replacing the approximate crack segment with an accurate region improves the calculation of the time-varying Finite Element (FE) stiffness matrix of the cracked shaft.

The diagnostic value of orbit shape analysis and its use to improve machine problem detection were investigated by Bachschmid et al. [9]. In their study, the full-spectrum analysis of rotating machine vibrations is a diagnostic instrument that may detect the signs of certain faults. The Shape and Directivity Index (SDI) of journal filtered orbits is a diagnostic measure that can be used in conjunction with full-spectrum analysis.

Prasad et al. [10] proposed the principal component analysis method for detection and localization of fatigue-induced transverse crack in shaft. Accelerated fatigue experiments using a customized setup are used to accomplish their research. Different vibration and strain sensor data were used in this investigation to extract time- and frequency-domain statistical characteristics. The vibration-based statistical features, which are sensitive to shaft transverse cracks, are presented in their article for various sensor kinds and mounting locations.

Abu-Mahfouz and Banerjee [15] demonstrated a novel procedure for crack detection and identification in a beam by using vibration signals and fuzzy clustering with an experimental setup. An electromagnetic shaker operated by an arbitrary function generator introduces excitation to the beam near its fixed end. Statistical moments, frequency spectra, and wavelet coefficients are used to examine the vibration signals for beam dynamic characteristics. These are then used as features in the fuzzy relational clustering process to split the data.

Both theoretically and experimentally, Douka and Hadjileontiadis [16] examined the

dynamic behavior of a cantilever beam with a breathing crack. Their primary goal is to use time-frequency approaches instead of Fourier analysis to reveal the system's nonlinear behavior. The instantaneous frequency is calculated using empirical mode decomposition and the Hilbert transform on both simulated and experimental response data. The instantaneous frequency variation follows specific patterns and can thus be used as a crack size indicator.

El-Mongy et al. [17] have presented the vibration analysis of a multi-fault transient rotor passing through sub-critical resonances. This research investigates the vibrational transient response of a cracked rotor in the presence of unbalance and coupling misalignment. The goal of this research is to look into the possibilities, benefits, and drawbacks of employing the sub-critical startup response to solve the fault identification problem. For different individual and multi-fault circumstances, numerical simulations employing finite element modelling and experimental studies are carried out.

By considering vibrations in the cross-section, Bovsunovskii [18] investigated the effect of crack depth and position on the vibration behavior of the cantilever beam. The first mode frequency of a cantilever beam with breathing crack (i.e. open and close crack) owing to longitudinal and bending force is calculated using the Rayleigh method.

2.2.2 Finite Element Method used for crack detection

Finite Element Analysis (FEA) is a sort of numerical examination approach that could be used to evaluate natural frequencies and mode shapes in 1D, 2D, and 3D examinations. Different researchers have employed different finite element analysis methodologies and software packages.

The dynamic behavior of a geared rotor-bearing system with a breathing crack was studied by Han et al. [19]. They employed the Finite Element Method (FEM) to build the slanted crack geared-rotor model, as well as the stress intensity factor based on fracture mechanics to calculate the slant crack's flexibility matrix. Hossain et al. [20] designed an experimental test rig for the vibration study of a cantilever beam partially

immersed in air and fluid medium, using a Polytech scanning vibrometer to quantify the vibration response. They've also forecasted the dynamic response of the same beam using the FEA method. The rheological properties of the viscous fluid are used to compare changes in the vibration response of the beam, such as frequency, amplitude, and resonance frequency.

The development of a FE approach and code for stability analysis of cracked functionally graded rotor-bearing systems in a thermal environment was presented by Gayen et al. [21]. In their study, translational and rotating inertia, gyroscopic moments, bending deformation, and material damping are all taken into account while modeling the functionally graded shaft with two-noded Timoshenko beam components. Their result shows that while the depth, locations, and orientation of cracks, as well as the material damping and thermal gradient, all affect the stability threshold speed, the material gradient index should be chosen carefully.

Using the finite element modeling of a rotor-bearing system, Sekhar [22] examined the dynamic behavior of the rotor carrying a double transverse crack. He's worked out how fracture factors like the slenderness ratio affect stability and eigen-frequencies. Silania et al. [23] investigated the dynamic behavior of a rotating shaft system with a breathing crack using the vibration analysis method. The stiffness matrix of the cracked element is computed using a modified integration approach. They used a FE formulation to describe the breathing crack, and frequency or time-domain methods to determine the rotor's vibration characteristics with the breathing crack.

Using a Kriging surrogate model, Lu et al. [24] suggested a super-harmonic feature-based updating technique for fracture detection in rotors. In their study for more sensitive and accurate breathing crack diagnosis, the nonlinear characteristics of breathing cracks from two places of the rotors are used instead of standard linear damage parameters. A FEM of a two-disc rotor-bearing system with a response-dependent breathing crack is also constructed, and experiments are partially confirmed. The relation between cracks and dynamic property changes was used by Abdo and Hori [25] to carry out numerical formulation fault detection in a structure. In this

research, the damaged region was discovered using the rotational features of mode shape. All of these investigations are conducted in the domain of finite element analysis.

Song et al. [26] created a new finite element model for three-dimensional FEA to investigate the behavior of a structure exposed to high-speed trains. Their goal was to improve FE models for use in railway bridge structural elements. Numerical samples of a simply supported steel concrete and a box-girder bridge structure were used to validate the derived finite element model.

Kim and Stubbs [27] developed a unique algorithm for fracture identification and quantification in structures based on changes in modal properties. With the information of pre and post-crack modal parameters, their technique was used to detect the crack in a two-span continuous structure. Chondros et al. [28] investigated the transverse vibration of a damaged beam with single and double edge open cracks using a continuously damaged beam vibration theory.

Using the FEM, Fotouhi [29] investigated the vibration analysis of a uniform cantilever beam with considerable deflection. For this investigation, he has established three goals. The first goal was to describe the problem's behavior as it transitioned from a linear to a nonlinear problem, and the second goal was to develop the finite element code for the problem. The third goal was to use a nonlinear dynamic analysis to explore the stability of a specific evenness position. They calculated the forces, stresses, strains, and time-varying displacements in the flexible beam as a result of different excitation loads.

2.2.3 Wavelet and Finite Element Methods for crack identification

In addition to the classical approaches, wavelet and FEA have been used to detect faults in cracked structures. This section describes a few of the research publications from this domain. The sensitivity of the wavelet technique in the identification of fractures in beam structures was researched and published by Quek et al. [30], taking into consideration the effects of various crack kinds, boundary conditions, and wavelet functions. Suh et al. [31] used a wavelet-based technique to investigate the non-linear

dynamic behavior of a model-based rotor with a transverse crack, which is effective in finding the mechanical chaotic response.

Loutridis et al. [32] developed a wavelet-based technique for detecting rapid changes in the spatial variations of the dynamic response of cracked structures, which was confirmed both analytically and experimentally. Using the FE approach of the B-spline wavelet on the interval, Xiang et al. [33] suggested a novel way for identifying the fracture size and position in the rotor using FEM of B-spline wavelet on the interval (BSWI). They used the BSWI Rayleigh-Timosinko beam element and the BSWI Rayleigh–Euler beam element to create the disc and slender shaft models, respectively. Qian et al. [34] used stress intensity factors in a finite element model to locate cracks in a damaged beam. This approach can also be used on complex structures that have cracks.

Ma et al. [35] developed a new wavelet-based beam element approach for analyzing difficult beams with irregular cross-sections and local loads. Using the Daubechies scaling element functions, they devised a Wavelet-based beam element approach. Gentile and Messina [36] suggested a continuous wavelet transform-based technique for determining the position of open cracks in damaged beams by minimizing the measurement data and the structure's baseline information.

To recognize crack location and size in beams, Li et al. [37] presented a wavelet FEM. They discretized the beam into a set of wavelet finite elements to accurately measure the vibration response (i.e. natural frequency) of the beam with various fracture sizes and locations.

2.2.4 Other approaches used for identification of crack

Sino et al. [38] investigated the dynamic behavior of a spinning composite shaft with internal damping using vibration analysis. They calculated the natural frequency and instability thresholds using a homogenized FE beam model that included internal damping, as well as comparing the urbanized simplified homogenized beam theory to the equivalent beam modulus theory. Stoisser and Audebert [39] proposed a theoretical

three-dimensional beam model with transverse crack, as well as a numerical and experimental method for crack identification in power plant rotational machinery.

The effect of a transverse crack in an orbital position of a cracked rotating shaft was investigated by Gomez et al. [40]. Shulzhenko and Ovcharova [41] gave a numerical investigation of the vibrational effects of a rotor's elastic axis braking with a transverse crack. Wang et al. [42] used the thin-walled structure theory to analyze the vibrations of a horizontal axis wind turbine. The forced response analysis is used to evaluate the stress-displacement field, dynamic displacement, and stress distribution of the wind tower blade rotor.

For identifying the crack depth and location in a rotor carrying a transverse crack, Dong et al. [43] suggested a wavelet finite element model and a high precision model parameter identification approach. Simultaneously, a novel method based on Laplace wavelets and empirical mode decomposition is being developed to get high precision model parameters, which will be used to improve crack recognition accuracy.

Experimental measurements of the natural frequencies and mode morphologies of revolving disk-blades-disk assemblies from a stationary frame were carried out by Presas et al. [44]. Experiments were carried out in this study to change the rotating speed of a disk-blade-disk assembly and to excite the spinning frame's first natural frequencies. Piezoelectric (PZT) patches from the revolving frame and a Laser Doppler Vibrometer are used to excite and measure the rotating structure (LDV). To explain the experimental results acquired from the stationary frame, a method to break down the structure's diametrical mode shapes into simple diametrical components (which determine the diametral mode shapes) was developed.

2.2.5 Artificial intelligence techniques based methods for crack detection

AI is defined as a machine's ability to mimic intelligent human behavior, to approximate traditionally defiant problems using human-inspired algorithms. AI techniques are an attempt to develop computer-based methods that could act like humans. They can have

the ability to execute tasks, learn languages, and imitate human expertise and decision-making.

Genetic Algorithm based identification of crack

A Genetic Algorithm (GA) is a type of evolutionary algorithm that falls into a larger category. It's a method of locating a rough solution to optimization and search problems.

Chou and Ghaboussi [45] developed a GA to solve an optimization issue for structural deterioration detection. To avoid structure analysis in fitness estimates, GA calculated deflections at unmeasured degrees of freedom. Peimani et al. [46] suggested a method for fault diagnostics based on GA and a cracked structural model. An analytical model of a cracked cantilever beam is used to represent the cracked-beam structure, and natural frequencies are produced using numerical methods. The location and depth of cracks in the cantilever beam are determined as an optimization problem, and genetic algorithms are utilized to minimize the cost function to determine the best location and depth. The experimental findings are also presented to validate the suggested approach and explore the modelling and measurement errors.

Shopova et al. [47] used GA to tackle a variety of problems. The number of selection, reproduction, and mutation parameters in the correspondence, genetic operators were introduced in a common genetic algorithm problem. Identification of a crack in beam using the frequency-based method and GA was studied by Mungla et al. [48]. Using single-input multi-output (SIMO) and Experimental Modal Analysis (EMA), the natural frequencies of the cracked and uncracked beams are measured. The frequency-based technique, as well as GA-based intelligent search for the same test locations, are used to detect the fracture position and severity using the measured frequencies of the beam with crack. The GA is used to locate the global minima of a fitness function that is a function of the cracked beam's measured and theoretical frequencies.

Pawar and Ganguli [49] developed a structural health monitoring mechanism for online

damage identification based on a genetic fuzzy system. For the fuzzy and genetic systems, they employed displacement and force-based measurement differences between damaged and undamaged conditions to generate the rules and data pool, respectively. The suggested technology was tested on composite rotor blades, with encouraging results.

Fuzzy Logic Method of crack identification

Fuzzy logic is a precise way to deal with uncertainty. Fuzzy inference is a method for interpreting values in an input vector and assigning them to an output vector based on a set of rules. To construct a fuzzy inference, rules must be used as inputs.

Based on FL and a Sugeno-style inference engine, Boutros and Liang [50] proposed a simple, effective, and robust fuzzy index fusion solution. This method has been successfully tested and validated in two different applications: milling tool condition monitoring and bearing condition assessment. According to their testing findings, the fused fuzzy index approach is sensitive to fault severity, capable of discriminating damages generated by a similar failure at various bearing components, but not subject to load variations.

According to Chandrashekhar and Ganguli [51], geometric and measurement uncertainty causes significant problems in damage assessment, which can be mitigated by utilizing FL-based technique for damage identification. Damage indicators are the curvature damage factor of a tapered cantilever beam and the damage indicator changes due to uncertainty in the geometric properties of the beam are studied using Monte Carlo simulation (MCS). According to their result, the approach can accurately identify both single and multiple cracks in the structure.

For model-based fault detection applications, Miguel and Blazquez [52] provide a fuzzy logic-based decision-making module. Fuzzy rules rely on the concept of fault possibility as well as knowledge of the residual equations' sensitivity and the fault size can be approximated with adequate accuracy using the experimental sensitivity values of the residual equations.

Sugumaran and Ramachandran [53] presented a method for diagnosing roller bearing faults utilizing a fuzzy classifier and histogram characteristics, with an emphasis on automatic rule learning. Their research discusses how to utilize a decision tree to pick the best few histogram features generated from vibration signals (bin ranges) to distinguish bearing fault scenarios from train samples. The results of building and testing a fuzzy classifier with representative data are positive and encouraging.

Artificial Neural Network-based identification of crack

In a variety of scenarios, neural networks have been successfully used to detect errors. An artificial neural network (ANN) is a network of interconnected natural or artificial neurons that processes data using a mathematical or computational model based on a connection approach to computation. It is made up of a vast number of nodes or neurons, which are simple processing elements. Each neuron simply computes a non-linear weighted sum of its inputs and sends the result to other neurons through its outgoing connections.

Kao and Hung [54] looked at a neural network based damage detection method that relied on changes in unknown structural systems' properties. This approach uses two systems: system identification and structural damage detection. System identification determines the uncracked and cracked states of structural systems. The dynamic response of a full-scale rotating shaft with three distinct crack depths was measured by Mohammed et al. [55]. The development and description of a revolutionary non-destructive system are presented. The system characterizes the system's behavior using parts of the Power Spectral Density (PSD) obtained from a rapid Fourier transform of the time history. The PSDs were fed into an ANN that exploited variations in the spectral content of the system's vibration to detect the presence of cracks. Chen et al. [56] developed a neural network-based structure fault isolation method that uses response data and transmissibility function as inputs to train the proposed network.

Saravanan et al. [57] used an ANN and Proximal Support Vector Machines (PSVM) to demonstrate the efficiency of wavelet-based features for fault diagnostics of a gearbox.

The J48 algorithm is used to classify statistical feature vectors derived from Morlet wavelet coefficients. From these, the dominating features were used to train and test ANN and PSVM, and their relative efficiency in classifying bevel gearbox problems was compared.

A method for identifying faults in the form of cracks and shaft misalignments has been proposed [58], which uses Variation Mode Decomposition (VMD) and probabilistic principal component analysis to denoise the vibration signals collected from a test rig, and then uses Convolutional Neural Networks (CNN) to extract signal features and classify the faults. To find cracks in the structure, Liu et al. [59] used a Back Propagation Neural Network (BPNN) along with computational mechanics. The method BPPN is used to assess the types of cracks present, their extent, location, and severity.

Mehrjoo et al. [60] presented their research on using a BPNN to estimate the damage intensities of joints for truss bridge systems. The neural network for crack identification was fed natural frequencies and mode shapes as input parameters. To demonstrate the correctness and efficiency of the proposed method, numerical example analyses on truss bridges are presented.

Hybrid techniques of crack identification

Various AI approaches, like fuzzy inference, neural networks, and genetic algorithms, have been hybridized in the development of crack detection approaches [49, 61, 62]. For problem identification of a spinning machine part, Firpi and Vachtsevanos [63] developed a genetically programmed artificial feature method. Using the genetically programmed artificial feature algorithm and vibration data as a source of information, they extracted artificial features. Agarwalla and Kumar [64] have applied a genetic fuzzy system for damage identification in cantilever beam structures. The proposed technique can reliably identify the crack positions and severity levels, according to the results obtained from the genetic fuzzy controller and experimental analysis.

2.3 Literature Summary

Several publications deal with the problem of detection, localization, and sizing of cracks. Using variations in natural frequencies, FRF amplitudes, and mode shapes, several researchers attempted to discover cracks in the structures, with varying degrees of success. Some researchers have described vibration-based methods that are necessary to understand the dynamics of the cracked structures which can be used for damage identification more efficiently. Most of the works are on a beam-like static structures. Because the coherence is generally good, modal analysis can be performed with a high degree of acceptance. AI approaches are a very efficient and precise tool for identifying crack locations that are extremely close to exact. AI can be used as a powerful device for online damage detection.

2.4 Research Gap

From the literature survey, it has been observed that damage can be assessed visually or by measuring frequency, mode shape, and structural damping. Visual inspection is a time-consuming method for detecting damage, and evaluating mode shape and structural deformation is more difficult than measuring frequency. Such metrics, on the other hand, are insufficiently sensitive to detect early flaws. As a result, other assisting parameters are required to improve the chances of detecting any minor flaw. Several researchers have developed several vibration-based methodologies that are required to understand the dynamics of cracked structures and can be utilized for more efficient damage identification, but not for damage localization. As a result, vibration-based damage detection methods urgently require some crack localization assisting strategies. Some methodologies are used in this work and have been carefully formulated for the problem definition to get at the desired solution. A single transverse crack was analyzed using theoretical and finite element analysis to obtain vibration parameters using various theories. The fuzzy logic algorithm is then constructed and developed utilizing these parameters as input while keeping the problem definition and variables in mind. The location and depth of a crack in a rotating shaft can be determined using this method.

Chapter 3

Vibration Analysis and Mathematical Modelling of Rotating Turbine Shaft

3.1 Introduction

Numerous techniques are available in the literature to detect the presence of a crack. In this chapter, the equation of motion and modelling of the rotor system and its components with and without the presence of crack is performed. Also, a logical approach has been adopted to develop the expression to calculate the natural frequency and phase shift of the turbine rotor shaft with the presence of a transverse crack. The developed expression or model is programmed in Matlab for the determination of vibration parameters. Finally, various crack locations and crack depths are taken to notice the change in natural frequency and phase shift of the shaft.

3.2 Vibration Differential Equations of Rotor Shaft

Rotor dynamics is a branch of applied mechanics which is used to analyze the diagnosis and behaviour of rotating machinery. Depending on the motion of the rotating structure, rotor dynamics are divided into; lateral (bending), longitudinal (axial), and torsional vibrations. Longitudinal vibration occurs if there is a compression and extension of the rotor. When the rotor oscillation motion twists the rotor, there is torsional vibration. A turbine shaft is a rotor-bearing system that consists the elements like; impeller, shaft, and linear stiffness bearings. Most hydro-turbines are bearing to bearing fixed configurations. So, in this study shafts with bearings at each end are considered. The

steps for the formulation of the equations of motion for rotating shaft using FEM are shown in Figure 3.1.

Thus, the overall differential equation will contain the bearing damping and stiffness, gyroscopic moments, rotary inertia effect, and transverse crack. For the turbine shaft, the loadings are in the transversal direction and most vibrations are in transverse and rotational directions. So in this study, only vibrations in the lateral direction (transverse and rotational displacements) are considered. Axial and torsional vibrations are omitted. This implies each node in an element has four degrees of freedom.

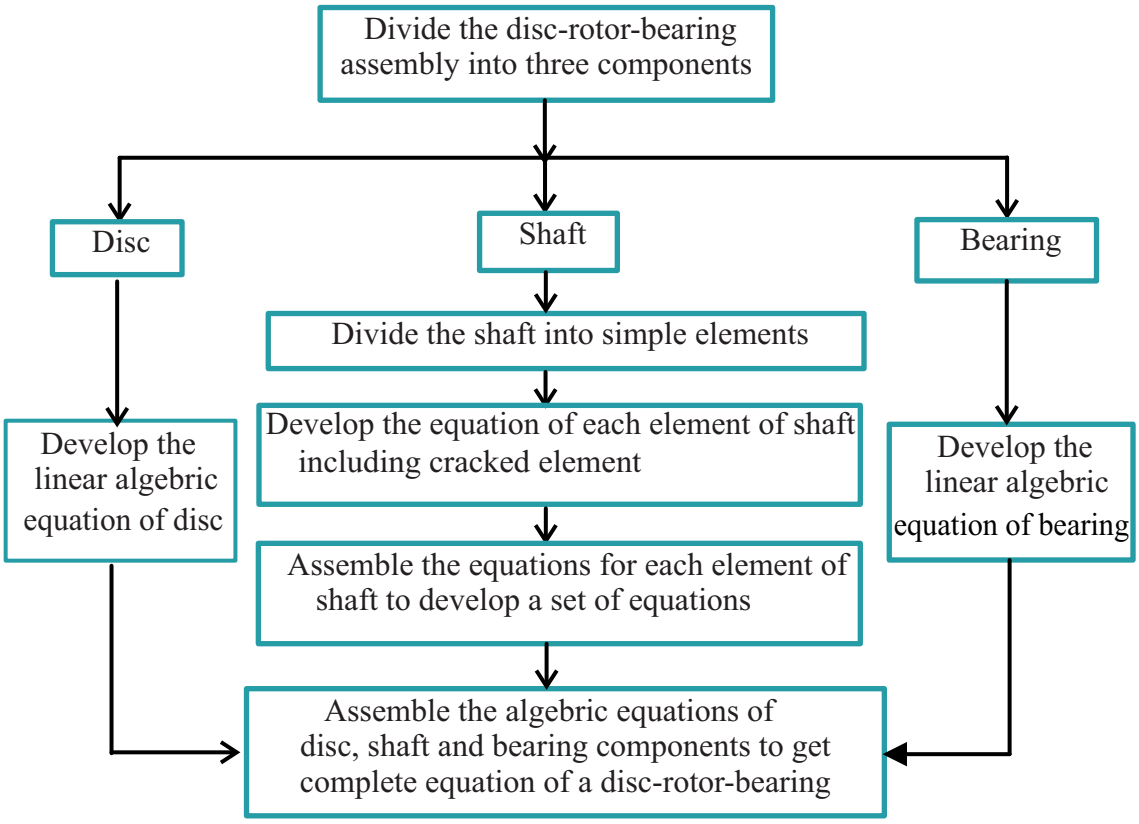

Figure 3.1: Steps for utilizing FEM to formulate the equations of motion for a rotating shaft

3.2.1 Bearings

Assume the bearings of the turbine shaft are linear and obey the following governing equation [65, 66]. The forces acting on the shaft as a result of the bearings are correlated with shaft displacements and velocities in this equation. The arrangement of the bearing-shaft-disc system is shown in Figure 3.2 below.

$$\begin{pmatrix} f_x \\ f_y \end{pmatrix} = -\begin{bmatrix} k_{uu} & k_{uv} \\ k_{vu} & k_{vv} \end{bmatrix}\begin{pmatrix} u \\ v \end{pmatrix} - \begin{bmatrix} c_{uu} & c_{uv} \\ c_{vu} & c_{vv} \end{bmatrix}\begin{pmatrix} \dot{u} \\ \dot{v} \end{pmatrix} \tag{3.1}$$

The vector notation of this equation is $Q_s = -K_b q - C_b \dot{q}$

where, $Q_s = \begin{pmatrix} f_x \\ f_y \end{pmatrix}$ *is the force vector*, $K_b = \begin{bmatrix} k_{uu} & k_{uv} \\ k_{vu} & k_{vv} \end{bmatrix}$ is the bearing stiffness and $C_b = \begin{bmatrix} c_{uu} & c_{uv} \\ c_{vu} & c_{vv} \end{bmatrix}$ is the bearing damping.

3.2.2 Impeller (Disc) Elements

The energy method is used to drive the element equation of motion of a typical rigid disc. Thus by considering the translational and rotational kinetic energy of the impeller (disc), the total kinetic energy of the disc is determined as follows [67].

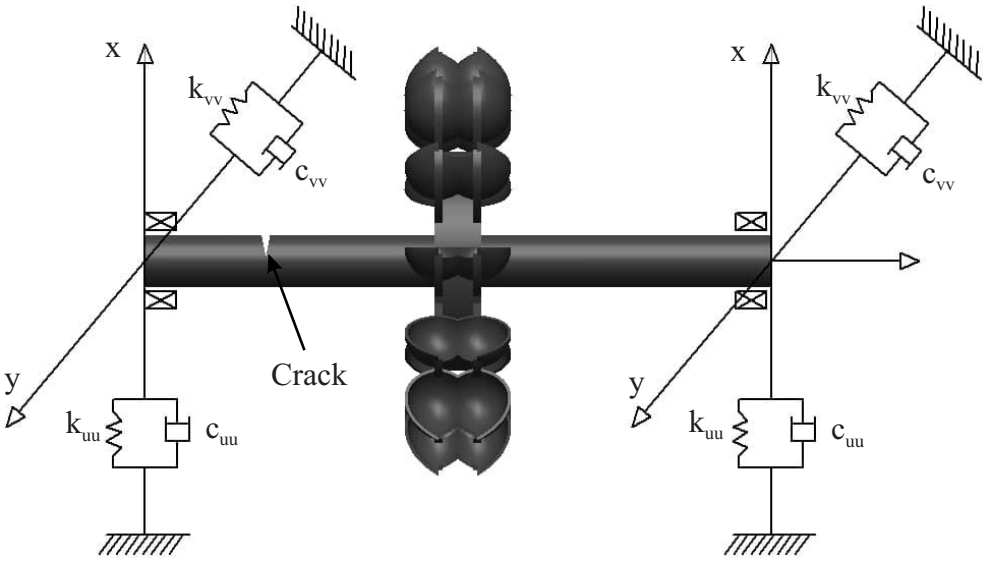

Figure 3.2: Arrangement of the disc-shaft-bearing system

$$T_d = \frac{1}{2}m_d\left(\dot{u}^2 + \dot{v}^2\right) + \frac{1}{2}I_d\left(\dot{\check{\theta}}^2 + \dot{\check{\psi}}^2\right) + \frac{1}{2}I_p\dot{\check{\emptyset}}^2 \tag{3.2}$$

In matrix form, it is expressed in the following way.

$$T_d = \frac{1}{2}\begin{pmatrix} \dot{u} \\ \dot{v} \end{pmatrix}^T \begin{bmatrix} m_d & 0 \\ 0 & m_d \end{bmatrix} \begin{pmatrix} \dot{u} \\ \dot{v} \end{pmatrix} + \frac{1}{2}\begin{pmatrix} \dot{\check{\theta}} \\ \dot{\check{\psi}} \\ \dot{\check{\emptyset}} \end{pmatrix}^T \begin{bmatrix} I_d & 0 & 0 \\ 0 & I_d & 0 \\ 0 & 0 & I_p \end{bmatrix} \begin{pmatrix} \dot{\check{\theta}} \\ \dot{\check{\psi}} \\ \dot{\check{\emptyset}} \end{pmatrix} \tag{3.3}$$

Where, $\dot{u}$ and $\dot{v}$ are the linear velocities in x and y directions and $\dot{\check{\theta}}$, $\dot{\check{\psi}}$ and $\dot{\check{\emptyset}}$ are the instantaneous angular velocities about the $\check{x}$, $\check{y}$, and $\check{z}$ directions respectively. m_d is the mass of the impeller or disc. Transformation matrix T is used to transform the displacements in a fixed frame of reference to rotating frames of reference and vice versa.

$$\{q\} = [T]\{p\} \tag{3.4}$$

$$\{q\} = \begin{pmatrix} u \\ v \\ \theta \\ \psi \end{pmatrix}, [T] = \begin{bmatrix} cos\emptyset & -sin\emptyset & 0 & 0 \\ sin\emptyset & cos\emptyset & 0 & 0 \\ 0 & 0 & cos\emptyset & -sin\emptyset \\ 0 & 0 & sin\emptyset & cos\emptyset \end{bmatrix}, \{p\} = \begin{pmatrix} \check{u} \\ \check{v} \\ \check{\theta} \\ \check{\psi} \end{pmatrix}$$

If the rotations are applied in new axes with the order of; ψ about y-axes, θ about x-axes and $\emptyset$ z-axes, So, the above angular velocities in equation (3.3) are expressed as;

$$\begin{pmatrix} \dot{\check{\theta}} \\ \dot{\check{\psi}} \\ \dot{\check{\emptyset}} \end{pmatrix} = \begin{pmatrix} 0 \\ 0 \\ \dot{\emptyset} \end{pmatrix} + \begin{bmatrix} cos\emptyset & -sin\emptyset & 0 \\ sin\emptyset & cos\emptyset & 0 \\ 0 & 0 & 1 \end{bmatrix} \begin{pmatrix} \dot{\theta} \\ 0 \\ 0 \end{pmatrix} + \begin{bmatrix} cos\emptyset & -sin\emptyset & 0 \\ sin\emptyset & cos\emptyset & 0 \\ 0 & 0 & 1 \end{bmatrix} \begin{bmatrix} 1 & 0 & 0 \\ 0 & cos\emptyset & sin\emptyset \\ 0 & -sin\emptyset & cos\emptyset \end{bmatrix} \begin{pmatrix} 0 \\ \dot{\psi} \\ 0 \end{pmatrix} \tag{3.5}$$

From this, the angle of rotation about the shaft is $\emptyset$. Assume the angular rotational speed of the disc is Ω. So the instantaneous angular velocity about the z-axes is $\dot{\emptyset} = \Omega$.

Then equation (3.5) becomes;

$$\begin{pmatrix} \dot{\check{\theta}} \\ \dot{\check{\psi}} \\ \dot{\check{\emptyset}} \end{pmatrix} = \begin{bmatrix} cos\theta & sin\emptyset cos\theta & 0 \\ -sin\emptyset & cos\emptyset cos\theta & 0 \\ 0 & -sin\theta & 1 \end{bmatrix} \begin{pmatrix} \dot{\theta} \\ \dot{\psi} \\ \Omega \end{pmatrix} \tag{3.6}$$

Thus, the total kinetic energy of the disc described in equation (3.2) above is rewritten as follows.

$$T_d = \frac{1}{2}m_d\left(\dot{u}^2 + \dot{v}^2\right) + \frac{1}{2}I_d\left(\dot{\theta}^2 + \dot{\psi}^2\right) + \frac{1}{2}I_p(\Omega^2 - 2\Omega\dot{\psi}) \tag{3.7}$$

By using Lagrange's Equation the element mass and gyroscopic matrices are obtained.

$$m_d^e = \begin{bmatrix} m & 0 & 0 & 0 \\ 0 & m & 0 & 0 \\ 0 & 0 & I_d & 0 \\ 0 & 0 & 0 & I_d \end{bmatrix}, and\ G_d^e = \begin{bmatrix} 0 & 0 & 0 & 0 \\ 0 & 0 & 0 & 0 \\ 0 & 0 & 0 & I_p \\ 0 & 0 & -I_p & 0 \end{bmatrix} \tag{3.8}$$

3.2.3 Shaft Elements

The turbine shaft is a rotating mechanical device with a central impeller that absorbs energy from fluid flow and converts it to useful work. The shaft will contribute stiffness, mass, and gyroscopic effects. In this study, the Bernoulli-Euler beam element theory is used to derive the elemental mass and stiffness matrices [68].

Bernoulli-Euler Beam Element Theory

The kinetic and strain energies in a beam are used to calculate the elemental stiffness matrices. Assuming the element translation is a cubic polynomial and satisfies the conditions at the nodes as:

$$u_e(0) = u_{e1}, \frac{\partial u_e}{\partial \xi}(0) = \psi_{e1}, u_e(l_e) = u_{e2}, \frac{\partial u_e}{\partial \xi}(l_e) = \psi_{e2} \tag{3.9}$$

Then the deflection of the element is approximated as follows.

$$u_e(\xi, t) = [N_{e1}(\xi) N_{e2}(\xi) N_{e3}(\xi) N_{e4}(\xi)] \begin{pmatrix} u_{e1}(t) \\ \psi_{e1}(t) \\ u_{e2}(t) \\ \psi_{e2}(t) \end{pmatrix} \tag{3.10}$$

where, $N_{ei}(\xi)$ are the shape functions and expressed as follows.

$$N_{e1}(\xi) = 1 - 3\frac{\xi^2}{{l_e}^2} + 2\frac{\xi^3}{{l_e}^3}, N_{e2}(\xi) = l_e(\frac{\xi}{l_e} - 2\frac{\xi^2}{{l_e}^2} + \frac{\xi^3}{{l_e}^3})$$

$$N_{e3}(\xi) = 3\frac{\xi^2}{{l_e}^2} - 2\frac{\xi^3}{{l_e}^3}, N_{e4}(\xi) = l_e(-\frac{\xi^2}{{l_e}^2} + \frac{\xi^3}{{l_e}^3}) \tag{3.11}$$

The beam element strain energy is given by [65];

$$U_e = \frac{1}{2}E_e I_e \int_0^{l_e} \left(\frac{\partial^2 u_e(\xi,t)}{\partial \xi^2}\right)^2 d\xi \tag{3.12}$$

Where, E_e is the material Young's modulus and I_e is the cross section's second area of the moment. When substituting the above equations, the strain energy of the element due to lateral displacement is;

$$U_e = \frac{1}{2}\begin{pmatrix} u_{e1}(t) \\ \psi_{e1}(t) \\ u_{e2}(t) \\ \psi_{e2}(t) \end{pmatrix}^T \begin{bmatrix} k_{11} & k_{12} & k_{13} & {}_k14 \\ k_{21} & k_{22} & k_{23} & k_{24} \\ k_{31} & k_{32} & k_{33} & k_{34} \\ k_{41} & k_{42} & k_{43} & k_{44} \end{bmatrix} \begin{pmatrix} u_{e1}(t) \\ \psi_{e1}(t) \\ u_{e2}(t) \\ \psi_{e2}(t) \end{pmatrix} \tag{3.13}$$

Where k_{ij} are the stiffness matrix elements described as shown.

$$k_{ij} = \frac{1}{2}E_e I_e \int_0^{l_e} N_{ei}''(\xi) N_{ej}''(\xi) d\xi \tag{3.14}$$

Where the second derivatives of shape functions N_{ei}'' and N_{ej}'' are described as;

$$N_{e1}'' = \frac{-6}{{l_e}^2}(1 - 2\frac{\xi}{l_e}), N_{e2}'' = \frac{2}{l_e}(-2 + 3\frac{\xi}{l_e})$$

$$N_{e3}'' = \frac{6}{l_e}(1 - 2\frac{\xi}{l_e}), N_{e4}'' = \frac{2}{l_e}(-1 + 3\frac{\xi}{l_e}) \tag{3.15}$$

Thus by substituting the above equations the stiffness matrix elements are developed. This implies the stiffness matrix of the element in a single bending plane is,

$$K_e = \begin{bmatrix} k_{11} & k_{12} & k_{13} & {}_k14 \\ k_{21} & k_{22} & k_{23} & k_{24} \\ k_{31} & k_{32} & k_{33} & k_{34} \\ k_{41} & k_{42} & k_{43} & k_{44} \end{bmatrix} = \frac{E_e I_e}{{l_e}^3} \begin{bmatrix} 12 & 6l_e & -12 & 6l_e \\ 6l_e & 4{l_e}^2 & -6l_e & 2{l_e}^2 \\ -12 & -6l_e & 12 & -6l_e \\ 6l_e & 2{l_e}^2 & -6l_e & 4{l_e}^2 \end{bmatrix} \tag{3.16}$$

Using kinetic energy, the mass matrix is obtained similarly with the elemental stiffness matrix with A_e denoting the cross-sectional area of the beam and ρ_e denoting material

density.

$$T_e = \frac{1}{2}\int_0^{l_e} \rho_e A_e \dot{u}_e^2(\xi,t)d\xi \tag{3.17}$$

By substituting the above shape functions, the kinetic energy becomes,

$$T_e = \frac{1}{2}\begin{pmatrix} \dot{u}_{e1}(t) \\ \dot{\psi}_{e1}(t) \\ \dot{u}_{e2}(t) \\ \dot{\psi}_{e2}(t) \end{pmatrix}^T \begin{bmatrix} m_{11} & m_{12} & m_{13} & m_{14} \\ m_{21} & m_{22} & m_{23} & m_{24} \\ m_{31} & m_{32} & m_{33} & m_{34} \\ m_{41} & m_{42} & m_{43} & m_{44} \end{bmatrix} \begin{pmatrix} \dot{u}_{e1}(t) \\ \dot{\psi}_{e1}(t) \\ \dot{u}_{e2}(t) \\ \dot{\psi}_{e2}(t) \end{pmatrix} \tag{3.18}$$

For a uniform cross-section, the above elements of the mass matrix are,

$$m_{ij} = \rho_e A_e \int_0^{l_e} N_{ei}(\xi) N_{ej}(\xi) d\xi \tag{3.19}$$

$$M_e = \begin{bmatrix} m_{11} & m_{12} & m_{13} & m_{14} \\ m_{21} & m_{22} & m_{23} & m_{24} \\ m_{31} & m_{32} & m_{33} & m_{34} \\ m_{41} & m_{42} & m_{43} & m_{44} \end{bmatrix} = \frac{\rho_e A_e l_e}{420} \begin{bmatrix} 156 & 22l_e & 54 & -13l_e \\ 22l_e & 4{l_e}^2 & 13l_e & -3{l_e}^2 \\ 54 & 13l_e & 156 & -22l_e \\ -13l_e & -3{l_e}^2 & -22l_e & 4{l_e}^2 \end{bmatrix} \tag{3.20}$$

Mass and Stiffness Matrices for Shaft Elements in Two Bending Planes

The stiffness and mass matrices in the two bending planes are;

$$K_e = \frac{E_e I_e}{{l_e}^3} \begin{bmatrix} 12 & 0 & 0 & 6l_e & -12 & 0 & 0 & 6l_e \\ 0 & -12 & -6l_e & 0 & 0 & -12 & -6l_e & 0 \\ 0 & -6l_e & 4{l_e}^2 & 0 & 0 & 6l_e & 2{l_e}^2 & 0 \\ 6l_e & 0 & 0 & 4{l_e}^2 & -6l_e & 0 & 0 & 2{l_e}^2 \\ -12 & 0 & 0 & -6l_e & 12 & 0 & 0 & -6l_e \\ 0 & -12 & 6l_e & 0 & 0 & 12 & 6l_e & 0 \\ 0 & -6l_e & 2{l_e}^2 & 0 & 0 & 6l_e & 4{l_e}^2 & 0 \\ 6l_e & 0 & 0 & 2{l_e}^2 & -6l_e & 0 & 0 & 4{l_e}^2 \end{bmatrix} \tag{3.21}$$

$$M_e = \frac{\rho_e A_e l_e}{420}\begin{bmatrix} 156 & 0 & 0 & 22l_e & 54 & 0 & 0 & -13l_e \\ 0 & 156 & -22l_e & 0 & 0 & 54 & -13l_e & 0 \\ 0 & -22l_e & 4{l_e}^2 & 0 & 0 & -13l_e & -3{l_e}^2 & 0 \\ 22l_e & 0 & 0 & 4{l_e}^2 & 13l_e & 0 & 0 & -3{l_e}^2 \\ 54 & 0 & 0 & 13l_e & 156 & 0 & 0 & -22l_e \\ 0 & 54 & -13l_e & 0 & 0 & 156 & 22l_e & 0 \\ 0 & 13l_e & -3{l_e}^2 & 0 & 0 & 22l_e & 4{l_e}^2 & 0 \\ -13l_e & 0 & 0 & -3{l_e}^2 & -22l_e & 0 & 0 & 4{l_e}^2 \end{bmatrix} \tag{3.22}$$

Gyroscopic Effects

The influence of the gyroscopic stiffening effect is one of the effects that separate the vibration of the rotor from other vibrations. Like disks, gyroscopic effects are generated in a shaft due to its high rotational speed and large polar moment of inertia [65].

$$T_{Ge} = \rho_e I_e \Omega \int_0^{l_e} \dot{\psi}_e(\xi,t)\theta_e(\xi,t)d\xi \tag{3.23}$$

From the above equation, the two bending planes are coupled with each other due to gyroscopic effects. The shape functions are determined as follows [66, 69];

$$\theta_e(\xi,t) = \frac{-dv_e}{d\xi}, \psi_e(\xi,t) = \frac{du_e}{d\xi} \tag{3.24}$$

And thus,

$$\begin{pmatrix} \theta_e(\xi,t) \\ \psi_e(\xi,t) \end{pmatrix} = \begin{bmatrix} 0 & -N_1' & N_2' & 0 & 0 & -N_3' & N_4' & 0 \\ N_1' & 0 & 0 & N_2' & N_3' & 0 & 0 & N_4' \end{bmatrix} q_e$$

$$\begin{pmatrix} \theta_e(\xi,t) \\ \psi_e(\xi,t) \end{pmatrix} = \begin{bmatrix} B_{11} & B_{12} & B_{13} & B_{14} & B_{15} & B_{16} & B_{17} & B_{18} \\ B_{21} & B_{22} & B_{23} & B_{24} & B_{25} & B_{26} & B_{27} & B_{28} \end{bmatrix} q_e \tag{3.25}$$

Where, $q_e = \begin{bmatrix} u_1 & v_1 & \theta_1 & \psi_1 & u_2 & v_2 & \theta_2 & \psi_2 \end{bmatrix}^T$ is the vector local node coordinates of the two bending planes. Thus by applying equation (3.25) into equation (3.23), the

above elemental kinetic energy due to gyroscopic effects becomes;

$$\boldsymbol{T_{Ge} = \dot{q}_e^T A q_e} \tag{3.26}$$

Where, $A_{ij} = -\rho_e I_e \Omega \int_0^{l_e} B_{2i}(\xi) B_{1j}(\xi) d\xi$

$\dot{q}_e = \begin{bmatrix} \dot{u}_1 & \dot{v}_1 & \dot{\theta}_1 & \dot{\psi}_1 & \dot{u}_2 & \dot{v}_2 & \dot{\theta}_2 & \dot{\psi}_2 \end{bmatrix}^T$ is the local coordinate's first derivative. Then, from Lagrange's equations

$$\begin{pmatrix} \frac{d}{dt}\left(\frac{\partial \boldsymbol{T_{Ge}}}{\partial \dot{q}_1}\right) - \frac{\partial \boldsymbol{T_{Ge}}}{\partial \boldsymbol{q_1}} \\ \vdots \\ \frac{d}{dt}\left(\frac{\partial \boldsymbol{T_{Ge}}}{\partial \dot{q}_8}\right) - \frac{\partial \boldsymbol{T_{Ge}}}{\partial \boldsymbol{q_8}} \end{pmatrix} = \left(A - A^T\right)\dot{q} = \Omega G_e \dot{q} \tag{3.27}$$

Thus the gyroscopic matrix elements are computed as follows.

$$G_{ij} = -2\rho_e I_e \int_0^{l_e} \left(B_{2i}(\xi) B_{1j}(\xi) - (B_{2j}(\xi) B_{1i}(\xi)\right) d\xi \tag{3.28}$$

By integrating the above equation, the elemental gyroscopic matrix in the two bending planes becomes;

$$G_e = \frac{\rho_e I_e}{15 l_e} \begin{bmatrix} 0 & 36 & 3l_e & 0 & 0 & 36 & -3l_e & 0 \\ -36 & 0 & 0 & -3l_e & 36 & 0 & 0 & -3l_e \\ 3l_e & 0 & 0 & 4{l_e}^2 & -3l_e & 0 & 0 & -{l_e}^2 \\ 0 & 3l_e & -4{l_e}^2 & 0 & 0 & -3l_e & {l_e}^2 & 0 \\ 0 & -36 & 3l_e & 0 & 0 & 36 & 3l_e & 0 \\ 36 & 0 & 0 & 3l_e & -36 & 0 & 0 & 3l_e \\ 3l_e & 0 & 0 & -{l_e}^2 & -3l_e & 0 & 0 & 4{e}^2 \\ 0 & 3l_e & {l_e}^2 & 0 & 0 & 3l_e & -4{e}^2 & 0 \end{bmatrix} \tag{3.29}$$

3.3 Assembly of Elemental Matrices and Boundary Conditions

The assembly of turbine elements is obtained by adding the elemental effects in their corresponding position. This means that the bearing effects are added at the two ends

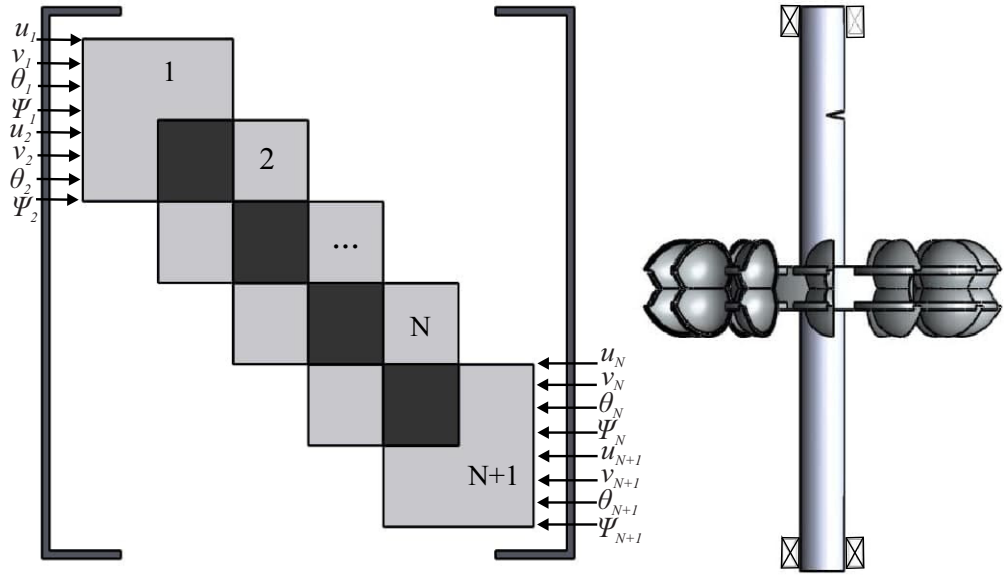

Figure 3.3: Assembly of matrices and boundary conditions

and disc effects are added at the middle of the shaft respectively. The global stiffness, mass, and gyroscopic matrices are obtained by overlapping their elemental matrices as shown in Figure 3.3 above. After completing the assembly of elemental matrices the equation constraints or boundary conditions are applied. The bearing flexibility is used to specify the boundary conditions. Since the supports are considered to be very stiff, the rotor cannot displace in the vertical and horizontal directions at the first node and the (N+1) node. As a result, the rows and columns in the global matrix that correspond to those nodes in the vertical and horizontal displacement must be deleted.

3.4 System Equations of Motion

By assembling the component equations, the full equation of motion becomes;

$$\boldsymbol{M\ddot{q}}(t) + (\boldsymbol{C} + \boldsymbol{\Omega G})\,\dot{\boldsymbol{q}} + \boldsymbol{K}\boldsymbol{q}(t) = \boldsymbol{Q_u} \tag{3.30}$$

Where, $\boldsymbol{q}(t) = \left[\boldsymbol{q_1^T} \ldots \boldsymbol{q_2^T} \ldots \boldsymbol{q_i^T} \ldots \boldsymbol{q_{N+1}^T}\right]^{\boldsymbol{T}}$ and $\boldsymbol{Q_u}$ are a 4(N+1) x 1 dimensioned nodal displacement vector and force vectors respectively. M, C, G, and K are the global mass, global damping, global gyroscopic, and global stiffness matrices of the rotor system respectively. Each matrix has dimensions of 4(N+1) x 4(N+1).

3.5 Finite Element Model of Cracked Rotor Shaft Systems

Basic Principle

The existence of a crack in a rotating shaft diminishes the structure's stiffness, hence lowering the natural frequencies and increasing the phase angle of the shaft's initial uncracked values. The reduction in stiffness is due to the reduction in area moment of inertia of cracked element. The area moment of inertia is a cross-sectional property that can be used to predict the bending and deflection resistance of beams. Beams having a large second moment of area are stiffer than those with a small second moment of area because they are more bending resistant.

The crack is assumed to be an initial angle ϕ concerning the fixed negative Y-axes at t=0. The hatched part in Figure 3.4 below defines the area of the crack segment [70–72]. From the figure, the centroidal coordinates are;

$$X_1(t) = -esin(\Omega t + \phi)$$

$$Y_1(t) = ecos(\Omega t + \phi) \tag{3.31}$$

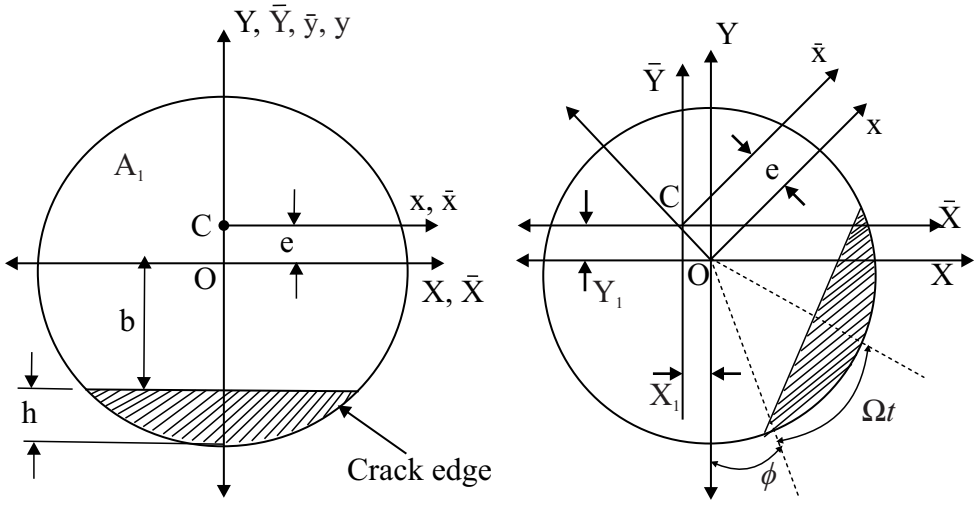

(a) Before rotation (b) After shaft rotation

Figure 3.4: Modelling diagrams of the cracked element cross-section [70–72]

The stiffness matrix of the cracked element k^i_{ce} is described as [73];

$$\boldsymbol{k^i_{ce}} = \frac{E_e}{{l_{ce}}^3}\begin{bmatrix} 12I_{\tilde{x}}(t) & 0 & 0 & 6l_{ce}I_{\tilde{x}}(t) & -12I_{\tilde{x}}(t) & 0 & 0 & 6l_{ce}I_{\tilde{x}}(t) \\ 0 & -12I_{\tilde{y}}(t) & -6l_{ce}I_{\tilde{y}}(t) & 0 & 0 & -12I_{\tilde{y}}(t) & -6l_{ce}I_{\tilde{y}}(t) & 0 \\ 0 & -6l_{ce}I_{\tilde{y}}(t) & 4{l_{ce}}^2I_{\tilde{y}}(t) & 0 & 0 & 6l_{ce}I_{\tilde{y}}(t) & 2{l_{ce}}^2I_{\tilde{y}}(t) & 0 \\ 6l_{ce}I_{\tilde{x}}(t) & 0 & 0 & 4{l_{ce}}^2I_{\tilde{x}}(t) & -6l_{ce}I_{\tilde{x}}(t) & 0 & 0 & 2{l_{ce}}^2I_{\tilde{x}}(t) \\ -12I_{\tilde{x}}(t) & 0 & 0 & -6l_{ce}I_{\tilde{x}}(t) & 12I_{\tilde{x}}(t) & 0 & 0 & -6l_{ce}I_{\tilde{x}}(t) \\ 0 & -12I_{\tilde{y}}(t) & 6l_{ce}I_{\tilde{y}}(t) & 0 & 0 & 12I_{\tilde{y}}(t) & 6l_{ce}I_{\tilde{y}}(t) & 0 \\ 0 & -6l_{ce}I_{\tilde{y}}(t) & 2{l_{ce}}^2I_{\tilde{y}}(t) & 0 & 0 & 6l_{ce}I_{\tilde{y}}(t) & 4{l_{ce}}^2I_{\tilde{y}}(t) & 0 \\ 6l_{ce}I_{\tilde{x}}(t) & 0 & 0 & 2{l_{ce}}^2I_{\tilde{x}}(t) & -6l_{ce}I_{\tilde{x}}(t) & 0 & 0 & 4{l_{ce}}^2I_{\tilde{x}}(t) \end{bmatrix} \tag{3.32}$$

where, $I_{\tilde{x}}$ and $I_{\tilde{y}}$ are the cracked element time-varying second moment of area about centroidal axes $\check{X}$ and $\check{Y}$ respectively.

Then, $I_{\tilde{x}}$ and $I_{\tilde{y}}$ are computed as;

$I_{\tilde{x}}(t) = I_x(t) - A_1 Y_1^2(t)$, then substitute the above equation and simplify.

$$I_{\tilde{x}}(t) = I_x(t) - \frac{1}{2}A_1 e^2[1 + \cos(2(\Omega t + \phi))] \tag{3.33}$$

$I_{\tilde{y}}(t) = I_y(t) - A_1 X_1^2(t)$, then substitute the above equation and simplify.

$$I_{\tilde{x}}(t) = I_y(t) - \frac{1}{2}A_1 e^2[1 - \cos(2(\Omega t + \phi))] \tag{3.34}$$

Where, A_1 is the cracked element left the uncracked area and e is the centroidal location of Y axes. I_x and I_y are the second moment of area of the cracked elements about X and Y axes.

$$\begin{aligned} A_1 &= \pi R^2 - A_c = \pi R^2 - R^2 cos^{-1}(1-\mu) - R^2(1-\mu)\sqrt{\mu(2-\mu)} \\ &= R^2\left(\pi - cos^{-1}(1-\mu) - (1-\mu)\sqrt{\mu(2-\mu)}\right) \end{aligned} \tag{3.35}$$

$e = \frac{2R^3}{3A_{ce}}\left(\sqrt{\mu(2-\mu)}\right)^3$, A_{ce} is the cracked element cross-sectional area and μ is crack depth ratio ($\mu = \frac{h}{R}$). R is the shaft radius and h is the crack depth.

Then,I_x and I_y are derived for $0 \le \mu \le 1$ as follows [71].

$$I_x = I - I_x^c = \frac{\pi R^4}{4} - \left(\frac{\pi R^4}{8} - \frac{R^4}{4}\left((1-\mu)\left(2\mu^2 - 4\mu + 1\right)\sqrt{\mu(2-\mu)} + sin^{-1}(1-\mu)\right)\right)$$

$$= \frac{\pi R^4}{8} + \frac{R^4}{4}\left((1-\mu)\left(2\mu^2 - 4\mu + 1\right)\sqrt{\mu(2-\mu)} + sin^{-1}(1-\mu)\right) \tag{3.36}$$

$$I_y = I - I_y^c$$

$$= \frac{\pi R^4}{4} - \frac{R^4}{12}\left((1-\mu)\left(2\mu^2 - 4\mu - 3\right)\sqrt{\mu(2-\mu)} + 3sin^{-1}\sqrt{\mu(2-\mu)}\right) \tag{3.37}$$

Without any crack, $I = \frac{\pi R^4}{4}$.

Thus, the time-varying moments $I_x(t)$ and $I_y(t)$ are defined as follows [73].

$$I_x(t) = \frac{I_x + I_y}{2} + \frac{I_x - I_y}{2}\cos(2(\Omega t + \phi)) - I_{xy}\sin(2(\Omega t + \phi)) \tag{3.38}$$

$$I_y(t) = \frac{I_x + I_y}{2} - \frac{I_x - I_y}{2}\cos(2(\Omega t + \phi)) + I_{xy}\sin(2(\Omega t + \phi)) \tag{3.39}$$

For the symmetrical cross-sectional area of a cracked element $I_{xy} = 0$. Thus, the cracked element time-varying second moments of area $I_{\tilde{x}}$ and $I_{\tilde{x}}$are determined.

$$I_{\tilde{x}} = I_1 + I_2\cos(2(\Omega t + \phi)) \tag{3.40}$$

$$I_{\tilde{y}} = I_1 - I_2\cos(2(\Omega t + \phi)) \tag{3.41}$$

where, I_1 *and* I_2 are constants with $I_1 = \frac{I_x + I_y - A_1 e^2}{2}$ and $I_2 = \frac{I_x - I_y - A_1 e^2}{2}$.

Thus the finite element stiffness matrix of the cracked element given in Equation 3.32 can be rewritten as follows.

$$k_{ce}^{i} = k_1^{i} + k_2^{i}\cos(2(\Omega t + \phi)) \tag{3.42}$$

where;

$$\boldsymbol{k_1^i} = \frac{E_e}{{l_{ce}}^3}\begin{bmatrix} 12I_1 & 0 & 0 & 6l_{ce}I_1 & -12I_1 & 0 & 0 & 6l_{ce}I_1 \\ 0 & -12I_1 & -6l_{ce}I_1 & 0 & 0 & -12I_1 & -6l_{ce}I_1 & 0 \\ 0 & -6l_{ce}I_1 & 4{l_{ce}}^2I_1 & 0 & 0 & 6l_{ce}I_1 & 2{l_{ce}}^2I_1 & 0 \\ 6l_{ce}I_1 & 0 & 0 & 4{l_{ce}}^2I_1 & -6l_{ce}I_1 & 0 & 0 & 2{l_{ce}}^2I_1 \\ -12I_1 & 0 & 0 & -6l_{ce}I_1 & 12I_1 & 0 & 0 & -6l_{ce}I_1 \\ 0 & -12I_1 & 6l_{ce}I_1 & 0 & 0 & 12I_1 & 6l_{ce}I_1 & 0 \\ 0 & -6l_{ce}I_1 & 2{l_{ce}}^2I_1 & 0 & 0 & 6l_{ce}I_1 & 4{l_{ce}}^2I_1 & 0 \\ 6l_{ce}I_1 & 0 & 0 & 2{l_{ce}}^2I_1 & -6l_{ce}I_1 & 0 & 0 & 4{l_{ce}}^2I_1 \end{bmatrix} \tag{3.43}$$

$$\boldsymbol{k_2^i} = \frac{E_e}{{l_{ce}}^3}\begin{bmatrix} 12I_2 & 0 & 0 & 6l_{ce}I_2 & -12I_2 & 0 & 0 & 6l_{ce}I_2 \\ 0 & -12I_2 & -6l_{ce}I_2 & 0 & 0 & -12I_2 & -6l_{ce}I_2 & 0 \\ 0 & -6l_{ce}I_2 & 4{l_{ce}}^2I_2 & 0 & 0 & 6l_{ce}I_2 & 2{l_{ce}}^2I_2 & 0 \\ 6l_{ce}I_2 & 0 & 0 & 4{l_{ce}}^2I_2 & -6l_{ce}I_2 & 0 & 0 & 2{l_{ce}}^2I_2 \\ -12I_2 & 0 & 0 & -6l_{ce}I_2 & 12I_2 & 0 & 0 & -6l_{ce}I_2 \\ 0 & -12I_2 & 6l_{ce}I_2 & 0 & 0 & 12I_2 & 6l_{ce}I_2 & 0 \\ 0 & -6l_{ce}I_2 & 2{l_{ce}}^2I_2 & 0 & 0 & 6l_{ce}I_2 & 4{l_{ce}}^2I_2 & 0 \\ 6l_{ce}I_2 & 0 & 0 & 2{l_{ce}}^2I_2 & -6l_{ce}I_2 & 0 & 0 & 4{l_{ce}}^2I_2 \end{bmatrix} \tag{3.44}$$

Therefore, the FE equation of motion of the rotor bearing-system with transverse open crack is written as;

$$M\ddot{q}(t) + (C + \Omega G)\,\dot{q(t)} + (\tilde{K} + K_1\cos(2(\Omega t + \phi)))\,q(t) = Q_u \tag{3.45}$$

where $\tilde{\boldsymbol{K}}$ is a stiffness matrix obtained by replacing the uncracked element stiffness matrix of the uncracked shaft by the cracked element stiffness matrix $\boldsymbol{K_1^i}$. $\boldsymbol{K_1}$ is another stiffness matrix; it has zero elements at all locations except at the cracked element location where the elements are equal to $\boldsymbol{K_2^i}$.

3.6 Dynamic Analysis and Response of the System

To determine the eigenvectors and eigenvalues of the rotor system, the second order differential equations of cracked and intact rotor shafts are changed into first order differential equations.

$$\begin{bmatrix} C + \Omega G & M \\ M & 0 \end{bmatrix}\frac{d}{dt}\begin{pmatrix} q \\ \dot{q} \end{pmatrix} + \begin{bmatrix} K & 0 \\ 0 & -M \end{bmatrix}\begin{pmatrix} q \\ \dot{q} \end{pmatrix} = \begin{pmatrix} 0 \\ 0 \end{pmatrix} \tag{3.46}$$

Substitute, $X = \begin{pmatrix} q \\ \dot{q} \end{pmatrix}$ and$\dot{X} = \frac{d}{dt}\begin{pmatrix} q \\ \dot{q} \end{pmatrix}$. Then this equation becomes; $A\dot{X} + BX = 0$,

where, $A = \begin{bmatrix} C + \Omega G & M \\ M & 0 \end{bmatrix}$ and $B = \begin{bmatrix} K & 0 \\ 0 & -M \end{bmatrix}$.

The solution is assumed in the form $x(t) = x_0e^{st}$ then $\dot{x}(t) = sx_0e^{st}$. Then substitute into

equation (3.46) [74].

$$sAx_0 = -Bx_0 \tag{3.47}$$

To determine the eigenvalues and corresponding eigenvectors of the rotor shaft, this equation is solved numerically in Matlab.

Using the rotational frequency in the shaft [75];

$$m\ddot{q} + c\dot{q} + kq = m\varepsilon\Omega^2 e^{j\Omega t}$$

$$\ddot{q} + 2\zeta\omega_n\dot{q} + {\omega_n}^2 q = \varepsilon\Omega^2 e^{j\Omega t} \tag{3.48}$$

Where; $\zeta = \frac{c}{2m\omega_n}$, $\omega_n = \sqrt{\frac{k}{m}}$, which is an undamped system natural frequency.

The harmonic response vector of the shaft is expressed as; $q = q_0 e^{j\Omega t}$.

Then the above equation becomes;

$$(-\Omega^2 + j2\Omega\zeta\omega_n + {\omega_n}^2)q_0 e^{j\Omega t} = \varepsilon\Omega^2 e^{j\Omega t}$$

$$q_0 = \frac{\varepsilon\Omega^2}{({\omega_n}^2 - \Omega^2) + j2\Omega\zeta\omega_n} = \frac{[\left({\omega_n}^2 - \Omega^2\right) - j2\Omega\zeta\omega_n]\varepsilon\Omega^2}{({\omega_n}^2 - \Omega^2)^2 + (2\Omega\zeta\omega_n)^2} \tag{3.49}$$

From this, it finds the magnitude of q_0

$$q_0 = \sqrt{\left(\frac{({\omega_n}^2 - \Omega^2)\,\varepsilon\Omega^2}{({\omega_n}^2 - \Omega^2)^2 + (2\Omega\zeta\omega_n)^2}\right)^2 + \left(\frac{-2\Omega\zeta\omega_n\varepsilon\Omega^2}{({\omega_n}^2 - \Omega^2)^2 + (2\Omega\zeta\omega_n)^2}\right)^2} \tag{3.50}$$

when simplifying

$$q_0 = \frac{\varepsilon\Omega^2}{\sqrt{({\omega_n}^2 - \Omega^2)^2 + (2\Omega\zeta\omega_n)^2}} \tag{3.51}$$

From this, the phase angle ϕ_p is given by:

$$\phi_p = tan^{-1}\left(\frac{2\Omega\zeta\omega_n}{({\omega_n}^2 - \Omega^2)}\right) \tag{3.52}$$

3.7 Numerical Result and Analysis

In this study, the FEM is used as a theoretical analysis method for the determination of crack signature parameters. For the determination of natural frequency and phase angle, the differential equation of the cracked and uncracked shaft has been programmed in Matlab. This method is the forward method. Table 3.1 below, shows the geometries and material parameters of the components of the turbine rotor. From the modal analysis of the rotor-disc-bearing system in Matlab, the following results are extracted.

Table 3.1: Geometry and material parameters of turbine shaft and its components

Parameters	**Shaft**	**Disk**
Parameters		
Material	Stainless steel	Stainless steel
Young's Modulus, E (Gpa)	*200*	*200*
Poisson's ratio, v	*0.3*	*0.3*
Density, ρ(Kg/m3)	*7800*	*7800*
Geometry		
Total length, L (m)	*0.715*	———
Outer diameter, Do (m)	*0.06*	*0.14*
Inner Diameter, Di (m)	———	*0.06*
Thickness, td (m)	———	*0.055*
Mass, m (Kg)	*15.621*	*26.314*

- *As illustrated in Figures 3.5, 3.6, 3.7 and 3.8, due to the formation of crack in the uncracked shaft, the natural frequency of the shaft decreases and corresponding phase angle increases. In addition, at the crack location, the mode shapes show distortions or sharp shifts.*

- *At the same location of the crack, as crack depth increases the natural frequency of the shaft decrease and corresponding phase angle increases, shown in Figures 3.9 and 3.10.*

- *Crack signature parameter values (frequency and phase angle) from the left and right sides of the impeller are symmetric with each other (see Figures 3.9 and 3.10*).

The first mode natural frequency and first mode phase angle of the uncracked shaft are 18.0403 Hz and 58.0006 degree respectively (depicted in Figure 3.5). By the formation of crack at the location of 268.2 mm with a dimensionless depth ratio

of 0.5, the first natural frequency decreased to 17.9365 Hz and the corresponding phase angle is increased to 58.2812 degree as illustrated in Figure 3.6. Similarly, as shown in Figures 3.7 and 3.8, the second mode natural frequency decreases, and the corresponding phase angle of shaft increases due to the formation of crack at the length of 268.2mm and dimensionless depth ratio of 0.5. This is due to the reduction in stiffness of the cracked element. Also Figures 3.6 and 3.8 illustrate that the mode shapes have distorted or exhibited abrupt alterations at crack locations. These distortions or alterations are due to the coupling of vertical and horizontal bending vibrations.

The effect of crack depth on change in natural frequency and change in phase angle was also analyzed as shown in Figures 3.9 and 3.10 below. From the analysis, it can be observed that while keeping the crack location constant when the crack depths are increased, the natural frequency of the shaft decreases. At the same condition, the corresponding phase angle of the cracked shaft increases. This is because of the reduction in stiffness of the cracked element. Also, it can be observed that while keeping the crack depth constant when the crack location varies from shaft end to middle span of the shaft, the natural frequency reduces and phase angle increases. This is due to shaft deflection and the gyroscopic effect of shaft and disk. The natural frequencies and phase angles of the shaft are changing with crack depth and crack location. Since there is no unbalanced force and misalignment in the shaft, the values of natural frequency and phase angle from the left and right sides of the mid-span of the shaft are symmetric. The half section natural frequency and phase angle data of the shaft are thus used to train the fuzzy logic algorithm for crack diagnosis.

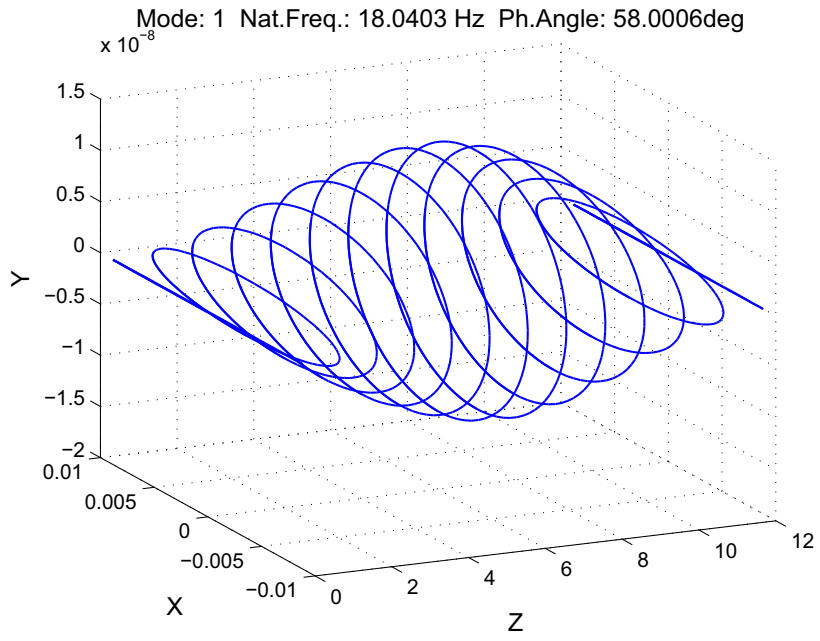

Figure 3.5: First mode results of the uncracked shaft

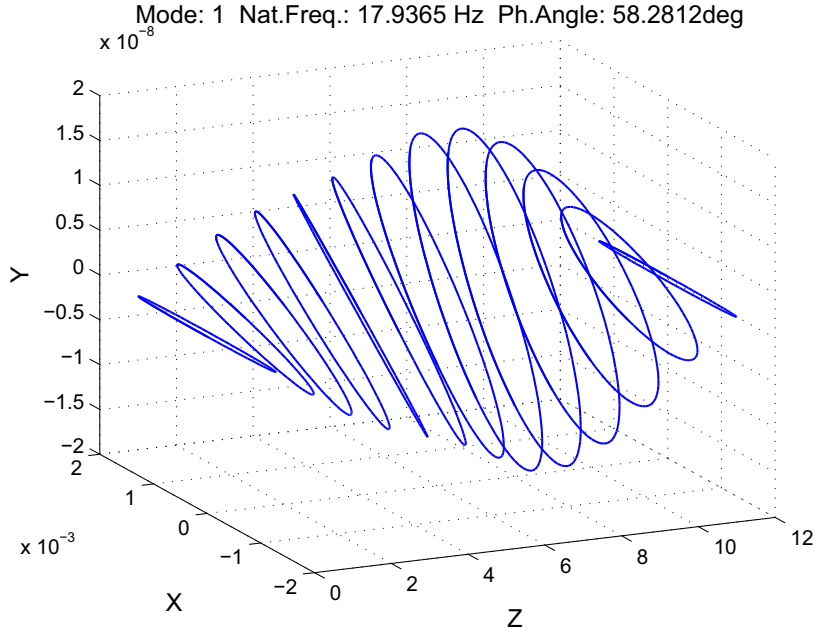

Figure 3.6: First mode results of the cracked shaft

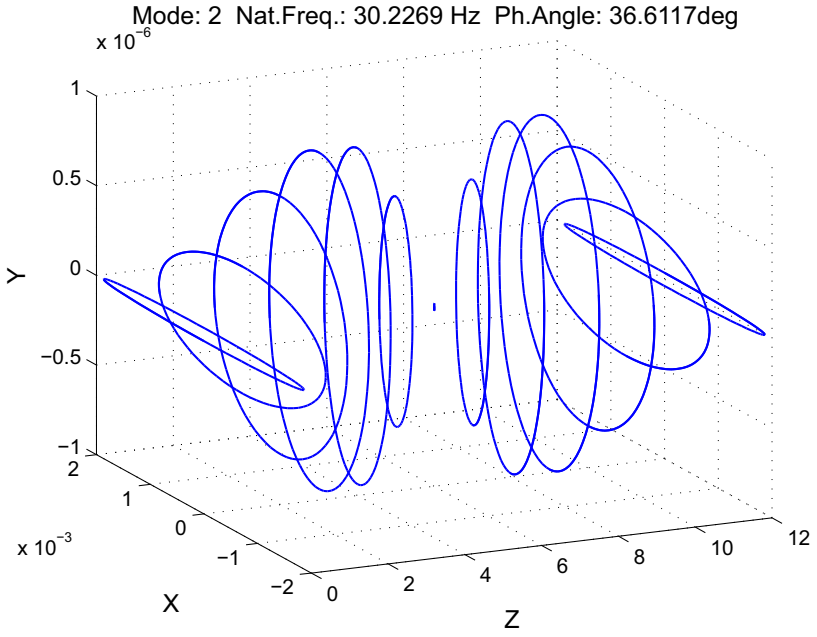

Figure 3.7: Second mode results of the uncracked shaft

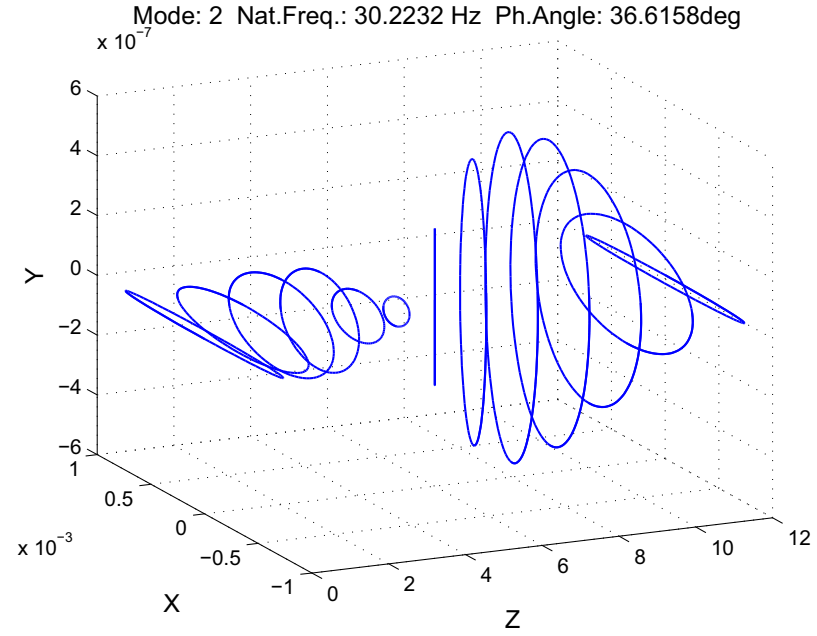

Figure 3.8: Second mode results of the cracked shaft

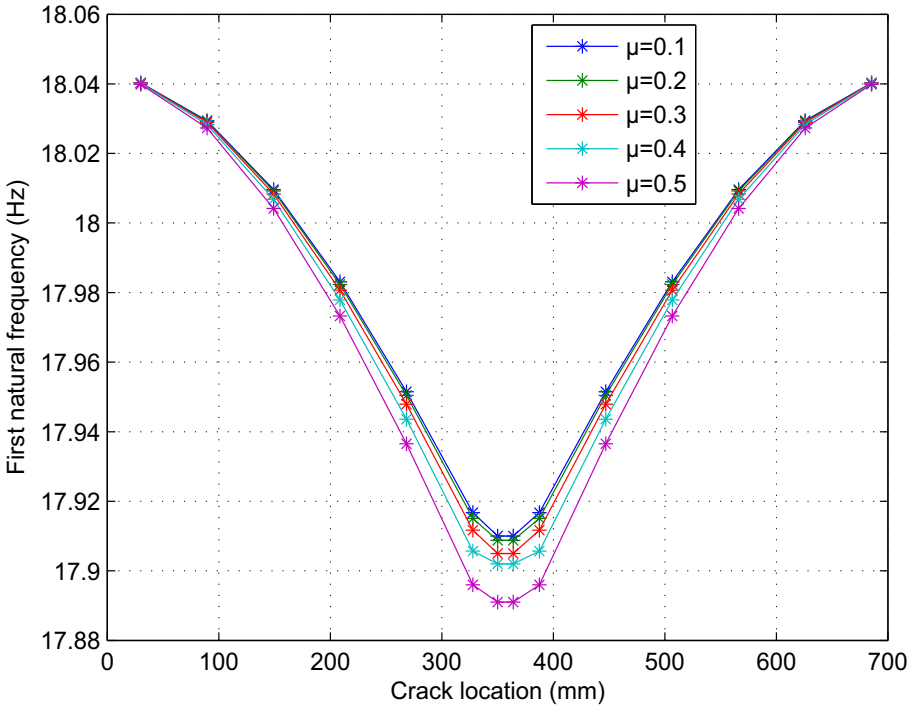

Figure 3.9: Characteristic curve for first mode frequency versus crack location at different depth ratios of crack

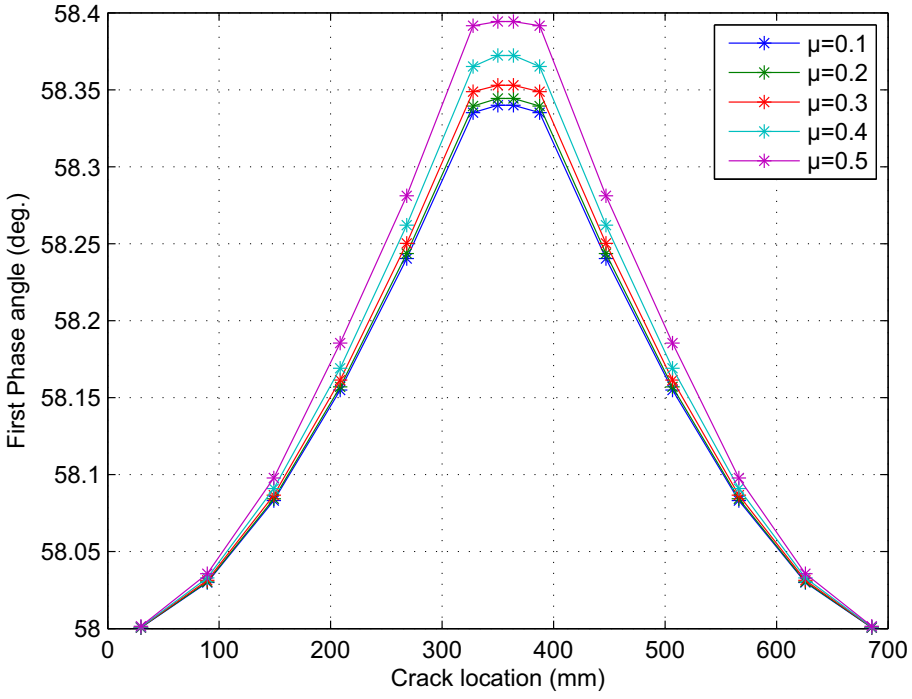

Figure 3.10: Characteristic curve for first mode phase angle versus crack location at different depth ratios of crack

Chapter 4

Finite Element Analysis of Turbine Rotor Shaft

4.1 Introduction

Finite element analysis is a powerful computational technique that allows simulating the physical behaviour of any structure by decomposing its domain into a finite number of subdivisions and converting it into a mathematical model [76]. These sub-domains, called elements, are connected by nodes, which specify the location in space where degrees of freedom and interaction between the elements exist. Modal analysis is a technique for describing a system's dynamic response in terms of its vibration modes. In a complex structure excitation signals and corresponding responses are difficult to measure or perceive. So, modal analysis converts these signals into modal parameters (natural frequency and mode shape) which can be straightforward to foresee. This implies that it extracts modal parameters from measured vibration data. In this chapter, modal analysis of cracked and uncracked turbine shafts is performed. For the cracked shaft, various crack locations and crack depths are taken to notice the change in the first two natural frequencies.

4.2 Finite Element Method using Ansys

The FEM simulates physical parts behaviour by dividing the geometry into many small parts (elements) of standard shapes. The analysis is carried out in Ansys software. This commercial software provides a wide range of modules, suitable to perform different

kinds of structural analysis. Corovic and Miljavec [77] used modal analysis and rotor dynamic theory to examine the mechanical vibrations of an interior permanent magnet synchronous electric motor intended for a wide range of speeds. Mechanical vibrations of the case study interior permanent magnet motor components were discovered and studied in their research using numerical, analytical, and experimental methods. Ansys Mechanical software, which is based on the FE approach, was used to do the numerical modal analysis and the rotor dynamic analysis (FEM).

For the current study, the modal analysis module was used to obtain the natural frequencies and mode shapes of the turbine shaft. The geometry of the turbine shaft was modelled in Solidwork premium and imported to the Ansys workbench. In this analysis, crack is formed at different locations of the shaft with different depths, and corresponding modal results are extracted.

4.3 Finite Element Analysis of Cracked and Intact Turbine Shaft in Ansys

To find change in behaviours of vibration parameters, the analysis of both cracked and intact shafts are performed in the frequency domain using Ansys software. The objective of this analysis is to evaluate the natural frequencies and mode shapes of both healthy and cracked turbine shafts.

4.3.1 Geometric modelling of shaft

The assessment for the modal analysis begins with the creation of a 3D solid model of the turbine shaft. The overall dimensions of the shaft and other components of the turbine are described in Table 3.1 of chapter three. Based on these dimensions the shaft is modelled in Solidwork premium with a diameter of 60mm and a length of 715mm.

4.3.2 Mesh generation and boundary conditions

The first step when performing the FEA is to discretize the domain of the structure into a finite number of elements. Such a procedure is known as meshing and largely defines the quality of the results of the simulation. Increasing the number of elements and nodes (what is known as a refined mesh) usually improves the accuracy of the simulation. After meshing the geometry, the boundary conditions of the body must be determined. The shaft has been fixed at both x and y directions (X=0, Y=0) and rotated at z-direction those are the parallel direction of the axis of the rotor. Rotor speed has been set to be constant, which is 600 rpm. For structural analysis, this usually means fixing one or more areas of the body. For meshing of the turbine shaft, a triangular element is used as shown in Figure 4.1 below. There are around 28,344 nodes and 14,480 elements.

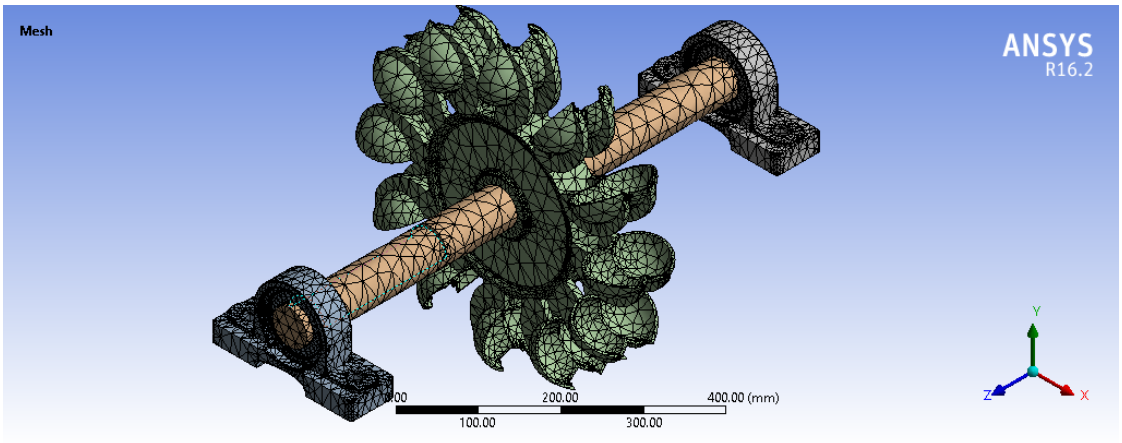

Figure 4.1: Meshed turbine shaft

4.4 Numerical Result and Analysis

The turbine shaft with and without crack has been simulated in the modal analysis of the Ansys workbench. Both shafts have rotated at 600rpm (10 Hz). From the modal analysis of the rotor-disc-bearing system in Ansys, the following results are extracted.

- *At the same location of the crack, as crack depth increases the natural frequency of the shaft decrease.*
- *At the same depth ratio of crack, the first and second mode natural frequency of the shaft are symmetric at shaft mid-span.*

As depicted in Figures 4.2 and 4.4, the first and second mode natural frequency values of the uncracked shaft are 22.979 Hz and 32.849 Hz respectively. By the formation of crack at a length of 268.2 mm (from the left bearing) with a dimensionless depth ratio of 0.5; the first natural frequency decreased to 17.017 Hz and the second mode natural frequency decreased to 32.686 Hz (see Figures 4.3 and 4.5). This is due to the reduction of the stiffness of the shaft's cracked element.

The characteristic curve of frequency versus the location of crack for different depth ratios is illustrated in Figure 4.6 below. This figure depicts that while keeping the crack location constant when the crack depths are increased, the natural frequency of the cracked shaft decreases. This is due to a decrease in the stiffness of cracked elements.

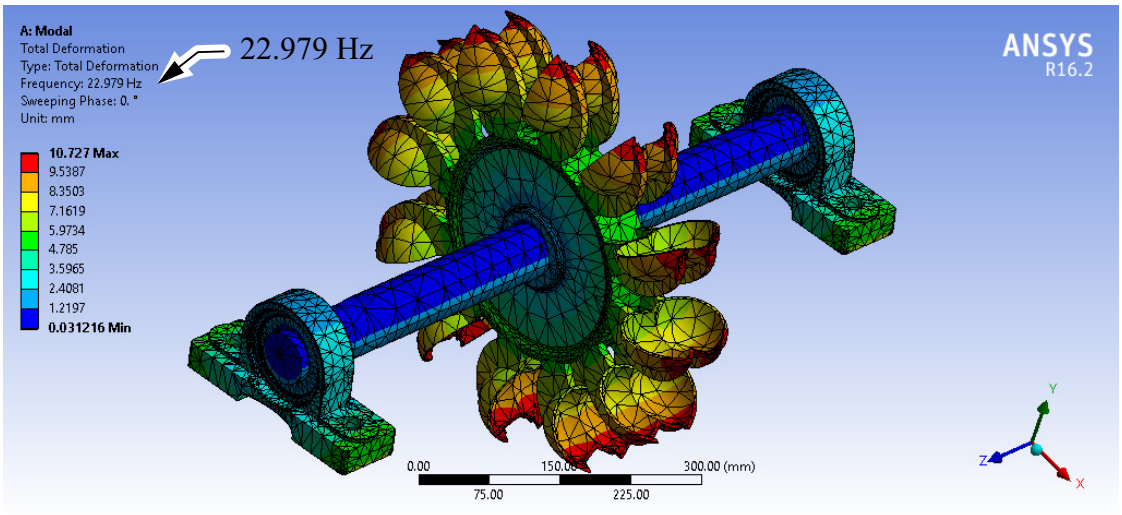

Figure 4.2: First mode results of the uncracked shaft

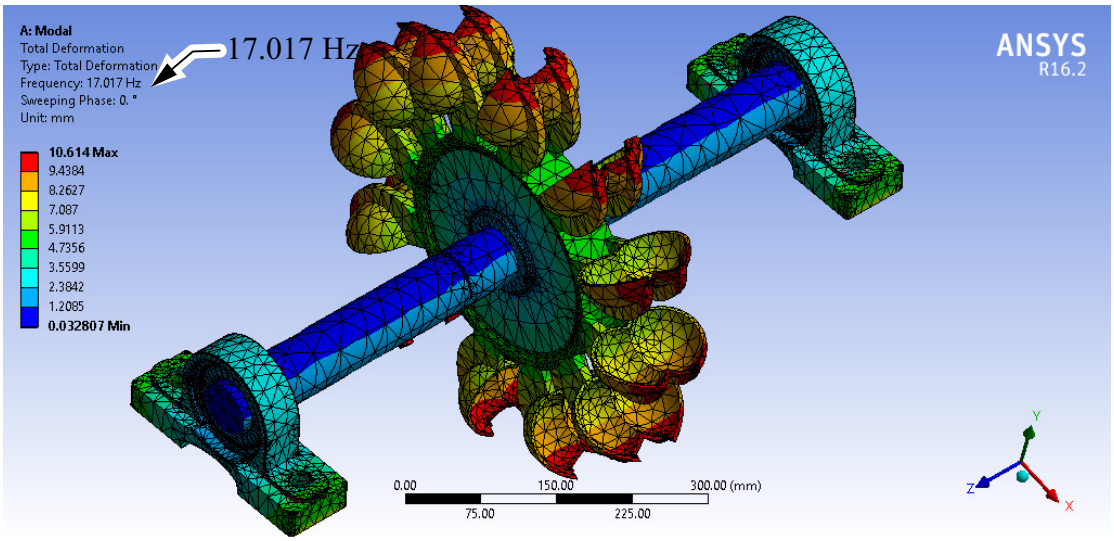

Figure 4.3: First mode results of the cracked shaft

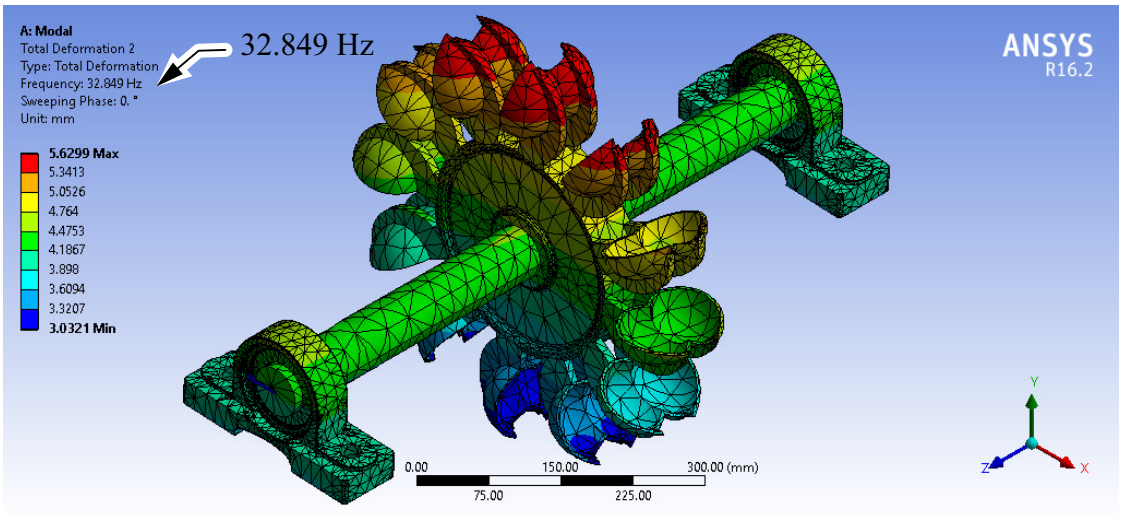

Figure 4.4: Second mode results of the uncracked shaft

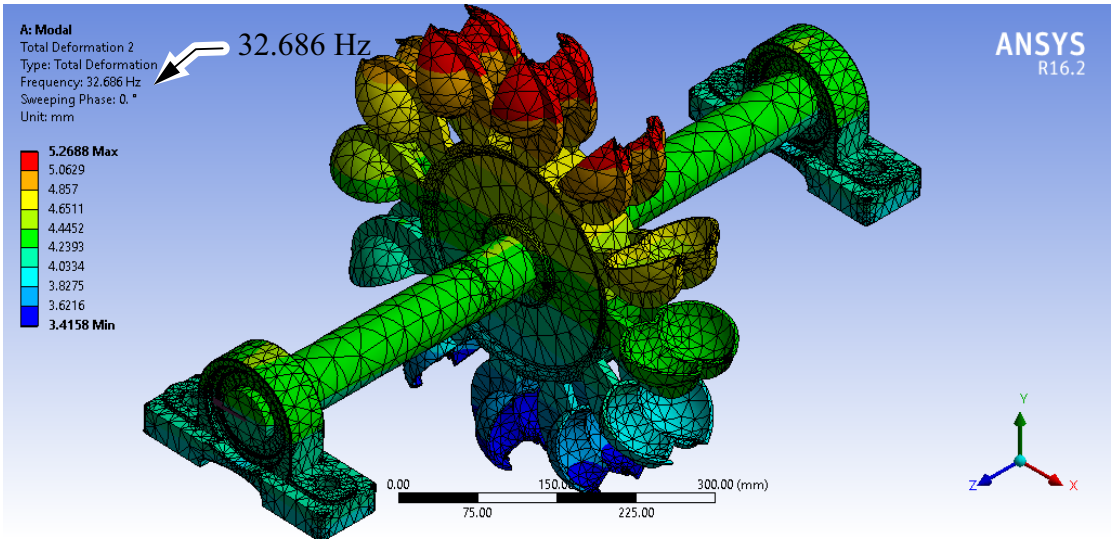

Figure 4.5: Second mode results of the cracked shaft

Also, it can be observed that while keeping the crack depth constant when the crack location varies from shaft end to middle span of the shaft, the natural frequency reduces. This is due to shaft deflection and the gyroscopic effect of the impeller or disk. The values of the natural frequency with equal distance from the left and the right side of the disk location are equal or symmetric. This is because of the absence of unbalance force and misalignment in the shaft. The half section natural frequency data of the shaft are thus used to train the fuzzy logic algorithm for crack diagnosis.

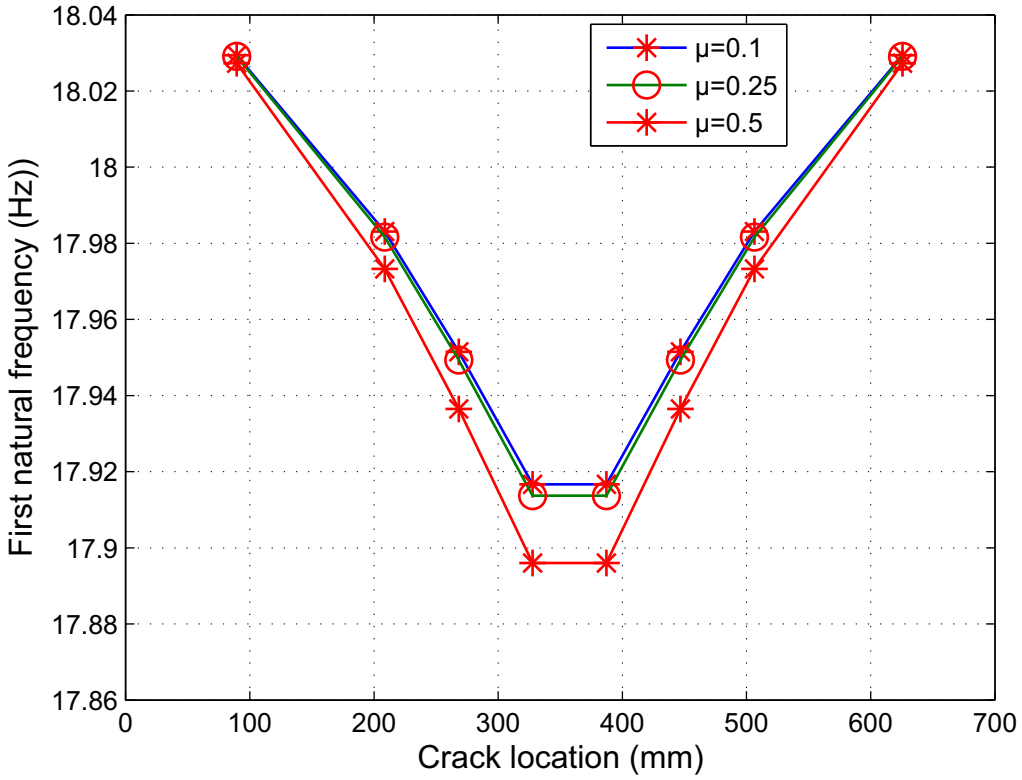

Figure 4.6: Characteristic curve for first mode natural frequency versus crack location at different crack depth ratios

Chapter 5

Fuzzy Logic Analysis for Crack Identification

5.1 Introduction

The presence of a crack in structures and machine components is a serious threat to the integrity of the system, which leads to reducing the life and may cause the failure of the system. Hence, an online method of crack detection is very essential. As seen in the previous two chapters, the change in vibration parameters are indicators of the presence of a crack in structures. In this chapter, an intelligent technique (fuzzy logic algorithm) is proposed to detect the location and depth of the crack in the shaft. The vibration parameters are used as input in this method, which is an inverse technique.

Fuzzy set concepts were first originated and proposed by Zadeh around 1965 [78, 79]. A membership function transfers the members of the universe into the unit interval, assigning degrees of belongingness to universe elements with regard to a set, and thereby characterizes a fuzzy set. Around 1975 Mamdani and Assilan [80] developed the Fuzzy Logic System (FLS) for the first time, which is a multi-value logic, which permits interval qualities to be characterized by linguistic expressions like true/false, high/low, yes/no. To use a more human-like way of thinking in computer programming, these evaluations can be mathematically expressed and processed by computers.

FL is a method of reasoning intended to model logical reasoning with vague or imprecise statements that resemble human reasoning. As explained and defined by

Zadeh [78, 79], FL provides a means of using approximate, inexact nature present in the real world problems and produce acceptable but definite output in response to incomplete, ambiguous, distorted, or inaccurate (fuzzy) input. The important part of the fuzzy logic FL is a set of linguistic control rules connected by the concept of fuzzy implication and fuzzy associative rules. The theory of fuzzy logic provides a mathematical foundation for reflecting the inherent ambiguities in human cognitive processes such as thinking and reasoning. The data is gathered from several partial facts in FL, and the consequences are predicted when it surpasses a certain threshold.

Based on the concept of fuzzy set theory, FL theory is a popular computing system and has been emerged as the most active area of research for several years. Time series prediction, pattern recognition, automatic control, expert systems, decision analysis, business, robotics, bioinformatics, and data classification are just some of the fields where this method is used. In literatures, Yu and Li [81], Azeem [82], Abdelazim and Malik [83], Trabelsi [84], and others have shown examples of fuzzy systems applications in identification, modelling, control, clustering, and filtering.

A FL controller works by applying fuzzy if-then rules and making decisions based on non-linear mapping of input data to a scalar output. As a result, any sensible number of inputs and outputs can be used. However, if more inputs and outputs are added, the rules may get more complicated. It is, therefore, preferable to divide the control system into smaller control units. The FLS can be used for uncertain or imprecise thinking, as well as non-linear systems that are difficult to model mathematically. FL is a set of linguistic control rules linked by the concepts of fuzzy implication and fuzzy associative rules, and it is an important aspect of FL. The terms utilized to design the fuzzy inference engine in the current work are listed in the following sections.

5.2 Concept of Fuzzy Sets and Membership Functions

The concept of a fuzzy set is an extension of the concept of a crisp set, in which it is specifically designed to mathematically represent the problem's uncertainty and vagueness. In 1993, Suzuki [85] attempted to give an analytical foundation for

the idea of fuzzy sets. A membership (characteristic) function is used to describe a fuzzy set, and it assigns a membership grade to each item that ranges from zero to one.

The **membership function** is a function that determines how much of a given input is part of a set. All operations on fuzzy sets are defined based on their membership functions because the membership function is the crucial component of a fuzzy set. A broad overview of many strategies for creating membership functions for fuzzy pattern recognition applications was provided by Medasani et al. [86].

Consider U to be a universal set and a fuzzy set on U is defined as;

$$\mu_F(\mathrm{x}) :\ \mathrm{U} \rightarrow [0, 1]$$

$$\mu_F is\ the\ membership\ function$$

$$\mu_F(x)\ is\ membership\ grade\ of\ x$$

The fuzzy set's nonzero degree membership elements are referred to as support, while the one-degree membership elements are referred to as a core. The fuzzy rules are used to determine the influence of the input membership functions on the fuzzy output sets of the final output conclusion. Membership functions are used to translate non-fuzzy input data to fuzzy linguistic terms and vice versa in the fuzzification and defuzzification procedures of a fuzzy logic system. Each input and output response has a different type of membership function. The trapezoidal, triangular, and Gaussian membership functions are mostly used in a FL analysis [87].

5.2.1 Triangular membership function

Let p, q, and r represents the x coordinates of the three vertices of $\mu_F(x)$ in fuzzy set F, as shown in Figure 5.1(a) below. The degree of membership is equivalent to zero at point 'p' and 'r' is equal to one at point 'q'. The mathematical exemplification of the

fuzzy triangular membership function $\mu_F(x)$ can be described below.

$$\mu_F(x) = \left\{ \begin{array}{cc} 0; & if\ x \leq p \\ \frac{x-p}{q-p}; & if\ p \leq x \leq q \\ \frac{r-x}{r-q}; & if\ q \leq x \leq r \\ 0; & if\ x > r \end{array} \right\} \tag{5.1}$$

5.2.2 Gaussian membership function

The Gaussian membership function is determined by the centre of membership functions (c) and width of the membership function (α) shown in Figure 5.1(b). The mathematical exemplification of the Gaussian fuzzy membership function can be described as below.

$$\mu_F(x : c, \alpha) = exp\left[-\frac{1}{2}\left(\frac{x-c}{\alpha}\right)^2\right] \tag{5.2}$$

5.2.3 Trapezoidal membership function

The trapezoidal membership function has the shape of a truncated triangular membership function. Let e, f, g, and h represent the x coordinates of the membership function. And then it has two base points (e, h) and two shoulder points (f, g) as shown in figure 5.1(c) below. The trapezoidal membership function is represented mathematically as follows.

$$\mu_F(x) = \left\{ \begin{array}{cc} 0; & if\ x \leq e \\ \frac{x-e}{f-e}; & if\ e \leq x \leq f \\ 1; & if\ f \leq x \leq g \\ \frac{h-x}{h-g}; & if\ c \leq x \leq d \\ 0; & if\ x \geq h \end{array} \right. \tag{5.3}$$

5.3 Fuzzy Inference System

A fuzzy inference system (FIS) is a framework or approach for mapping a set of fuzzy rules to an output. The mapping then serves as a foundation for making decisions and identifying patterns. FIS evaluates imprecision and ambiguity by employing appropri-

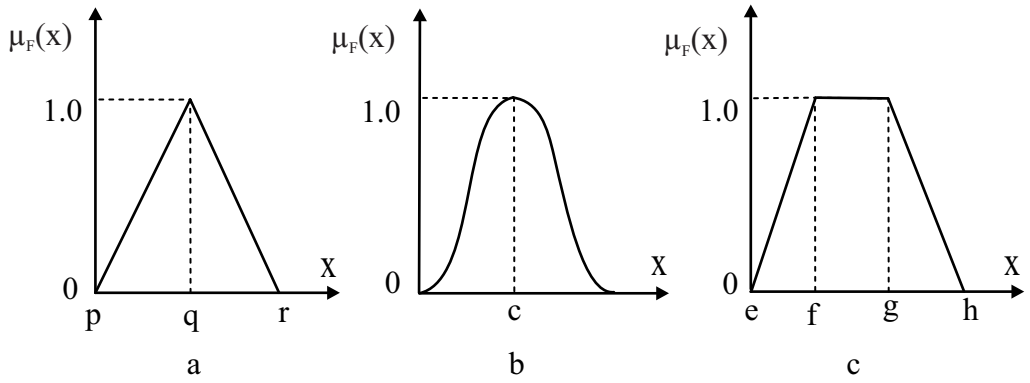

Figure 5.1: Membership functions used in FLS analysis
(a) Triangular (b) Gaussian and (c) Trapezoidal

ate rule bases to characterize the fuzziness of real-world data. For FIS, membership functions, fuzzification, and defuzzification are the main building blocks. There are two types of FIS. These are Mamdani type FIS and Sugeno type FIS.

Mamdani inference system

The output membership functions of a Mamdani-type inference system are often fuzzy sets. Each output variable has a fuzzy set that must be defuzzified after the aggregation procedure is completed.

Sugeno inference system

In many ways, Sugeno FIS is comparable to the Mamdani approach. Fuzzifying the inputs and applying the fuzzy operator are the first two steps of the fuzzy inference process. Sugeno output membership functions are either linear or constant, which is the fundamental distinction between Mamdani and Sugeno.

5.3.1 Fuzzy linguistic variables

A linguistic variable is a variable in a natural or artificial language that is made up of words or sentences rather than numbers and has related degrees of membership. Zadeh [88] proposed the concept of linguistic and fuzzy variables in 1965. These variables are the objectives that try to define the variable range. For instance, Speed is a linguistic variable with values such as slow, fast, very fast, and so on.

5.3.2 Fuzzy controller/ Fuzzy If-then rules

FL controllers employ fuzzy rules instead of equations to control systems. In FL, fuzzy rules are a set of linguistic statements that have been supported as a fundamental instrument for articulating pieces of knowledge. As described by Zadeh [88], fuzzy controllers use terms of linguistic variables to link the input variables with outcome variables. Hence, the antecedents and consequences of fuzzy if/then rules are fuzzy rather than crisp. As a result, the most important prerequisite for the FL foundation is a collection of fuzzy if/then rules.

The fuzzy mechanism's rules are usually written in this format: *If (input 1 is membership function 1) and/or (input 2 is membership function 2) and/or .... Then (output n is output membership function n).*

For example; if the distance from the obstacle is near and the angle from the obstacle is small, then turns very sharply. This is a rule used to control the steering system of the robot in the robot navigation system for obstacle avoidance. There would have to be membership functions that define what we mean by the *obstacle is near* (input 1), *small-angle* (input 2) and *turn very sharply* (output 1). For the particular control system, the output is controlled by the If-Then rules on the input. The development of fuzzy logic controller consists of Fuzzification, Rule evaluation and Defuzzification [89]. Simple architecture for a fuzzy logic controller is shown in Figure 5.2 below.

Fuzzification

Fuzzification is defined as the process of converting precise data into imprecise data or transforming a crisp set to a fuzzy set. This procedure essentially converts precise crisp

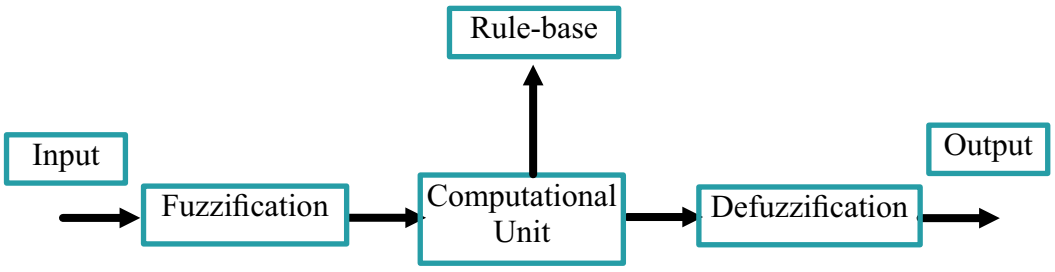

Figure 5.2: Fuzzy controller architecture

input values into linguistic variables [90]. The crisp value is fuzzified by using if-then rules. As an illustration, consider the following: (If the distance from the obstacle is near and the angle from the obstacle is small, then turn very sharply). The process of taking an input such as distance and processing it through a membership function to determine what we mean by distance is *"near"* is called fuzzification.

Rule base

Rule base or rule evaluation is the main computational unit that processes the input fuzzy values and computes the output fuzzy values [89].

Defuzzification

Defuzzification is the process of converting imprecise data into precise data or the process of reducing a fuzzy set into a crisp set or converting a fuzzy member into a crisp member. It is the inverse of fuzzification. There are two common methods for defuzzification [91].

i. **Centroid method:** this method is also known as the centre of gravity or the centre of area method. It is the most commonly used method and it obtains the centre of the area (x*) occupied by the fuzzy set. It is computationally difficult for sophisticated membership functions. The centroid defuzzification technique can be expressed as;

$$x^* = \frac{\int \mu_F(x) x dx}{\int \mu_F(x) dx}; for\ continues\ membership\ function$$

$$x^* = \frac{\sum_{i=1}^{n} x_i \mu_F(x_i)}{\sum_{i=1}^{n} \mu_F(x_i)}; for\ discrete\ membership\ function \tag{5.4}$$

where; n is the number of elements,x_i's are the elements and $\mu_F(x_i)$ is the membership function.

ii. **Mean of maxima (MOM) method:** this is one approach to difuzzify the output , which involves taking the crisp value with the highest degree of membership. Several elements are having the maximum value, the mean value of the maxima is

taken. This difuzzification method is expressed as;

$$x^* = \frac{\sum_{x_i \in M} x_i}{|M|} \tag{5.5}$$

$$Where;\ M = \left\{ x_i \middle| \mu_F(x_i)\ is\ equal\ to\ height\ of\ fuzzy\ set \right.$$

$$|M|\ is\ the\ cardinality\ of\ set\ M$$

$$M = \left\{ x_i \in [-c, c] \middle| \mu_F(x_i)\ is\ equal\ to\ height\ of\ fuzzy\ set \right.$$

5.4 Fuzzy Logic Mechanism for Crack Identification in a Shaft

5.4.1 Training methodology

Different methods have been used to construct fuzzy systems from data automatically. In this thesis cluster analysis is used. Cluster analysis is a data classification approach that divides data into groups or clusters. Each data must be assigned to one of the classes in this analysis. It's feasible to learn fuzzy if-then rules from data by applying fuzzy clustering methods. To train the fuzzy logic algorithm for identification purposes first and second mode results are proposed. The input parameters for identifying the location and depth of the crack are the first and second natural frequency and corresponding phase angle of the shaft. These crack signature parameters are obtained from previous theoretical analyses. Thus, the proposed FIS has four input and two output parameters. Then to assign the membership functions and linguistic variables, the obtained data's are arranged in different classes or ranges. The following are the natural linguistic representations used for the inputs and the outputs.

First natural frequency = 'fnf'
First phase angle ='fpa'
Second natural frequency ='snf'
Second phase angle ='spa'
Crack location ='cl'

Crack depth ratio='cdr'

Then the fuzzy rules are defined in the following general form: If (fnf is F_i and fpa is PA_j and snf is f_k and spa is pa_l) then (cdr is CD_{ijk} and cl is CL_{ijk}). Where, i, j, k, and l are a number of membership functions with i= 1 to 26, j=1 to 26, k=1 to 26, l=1 to 26. This is because of 'fnf', 'fpa', 'snf', and 'spa' have 26 membership functions each.

The crisp values of relative crack location and relative crack depth are determined using the center of gravity approach, as described by Das and Parhi [92].

$$W_{ijk} = \mu fnf_i(freq_i) \wedge \mu fpa_j(phan_j) \wedge \mu snf = k(freq_k) \wedge \mu spa(phan_l) \tag{5.6}$$

Where freqi, phanj, freqk, and phanl are the first natural frequency, first phase angle, second natural frequency and second phase angle respectively. The membership values of the crack location and crack depth are calculated using the composition rule of inference proposed by Das and Parhi [92].

$$\mu_{cl_{ijkl}}(location) = W_{ijkl} \ \wedge \mu_{cl_{ijkl}}(location) length\ CL \tag{5.7}$$

$$\mu_{cd_{ijkl}}(depth) = W_{ijkl} \ \wedge \mu_{cd_{ijkl}}(depth) depth\ CD \tag{5.8}$$

The following is the general conclusion that may be written by merging the output of all the fuzzy:

$$\mu_{cl_{ijkl}}(location) = \mu_{cl_{1111}} \vee \cdots \vee \mu_{cl_{ijkl}}(location) \vee \cdots \vee \mu_{cl_{26262626}}(location) \tag{5.9}$$

$$\mu_{cd_{ijkl}}(depth) = \mu_{cd_{1111}} \vee \cdots \vee \mu_{cd_{ijkl}}(depth) \vee \cdots \vee \mu_{cd_{26262626}}(depth) \tag{5.10}$$

The crisp values of crack location and crack depth are determined using the center of gravity approach, as described by Das and Parhi [92].

$$Crack\ location = \frac{\int location.\mu_{cl}(location).d(location)}{\int \mu_{cl}(location).d(location)} \tag{5.11}$$

$$Crack\ depth = \frac{\int depth.\mu_{cd}(depth).d(depth)}{\int \mu_{cd}(depth).d(depth)} \tag{5.12}$$

5.4.2 Fuzzy Logic controller for crack identification

As shown in Figure 5.3 below, the first natural frequency, first phase angle, second natural frequency, and second phase angle of the shaft are input data for the fuzzy controller, whereas crack location and crack depth are output parameters. To train the fuzzy controller, many hundred fuzzy rules are outlined. Figure 1 of Appendix A lists some of the fuzzy rules from a total of several hundred fuzzy rules. The rule base and the input data were used to generate the output data. The fuzzy logic controller in this work was constructed utilizing three types of membership functions: triangular, trapezoidal, and Gaussian membership functions. Figure 2 of Appendix A illustrates the operation and method of fuzzy cluster analysis for crack identification.

There are a total of twenty-six membership functions for each input parameter, seven membership functions for crack location, and six membership functions for crack depth. Comparison of the results obtained from theoretical and fuzzy controllers using triangular membership functions, trapezoidal membership functions, and Gaussian membership functions are described in chapter seven.

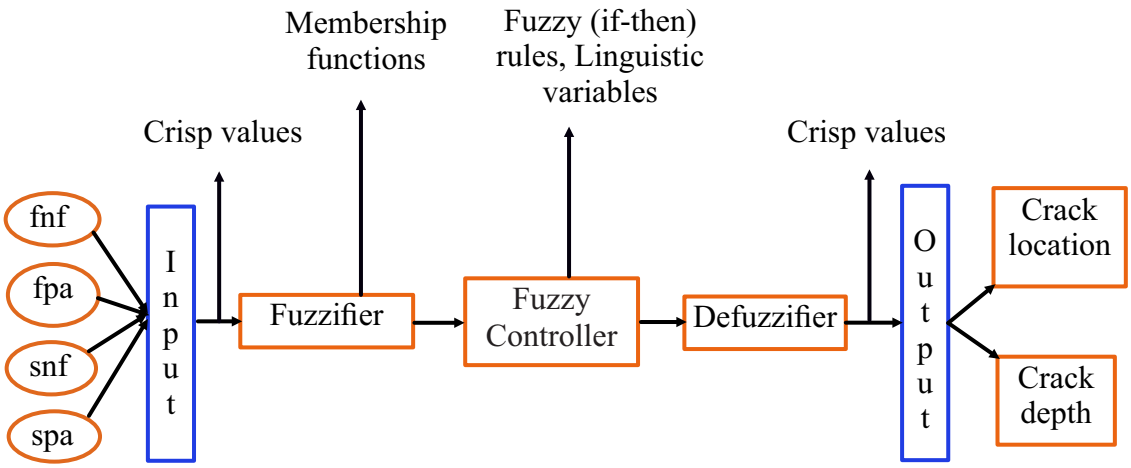

Figure 5.3: Schematic diagram of fuzzy inference system for crack identification

5.4.3 Simulink model for crack identification

As described above the fuzzy logic controller with three different membership functions has four input and two output parameters. So, for the easiness of the determination of output parameters Simulink model is designed. This model shows the values of output parameters from the three different fuzzy controller membership functions at a time. Figure 5.4 below shows the proposed Simulink model for the identification of crack.

5.4.4 Why Fuzzy Logic is used

- Does not require mathematical formulation.
- Powerful tool for dealing with imprecision, uncertainty.
- Precision in FL is exchanged for tractability, resilience, and a low-cost solution.
- Provides the ability to use FL when appropriate with other control techniques.
- Offers a fuzzy inference engine that can run the fuzzy system on its own.

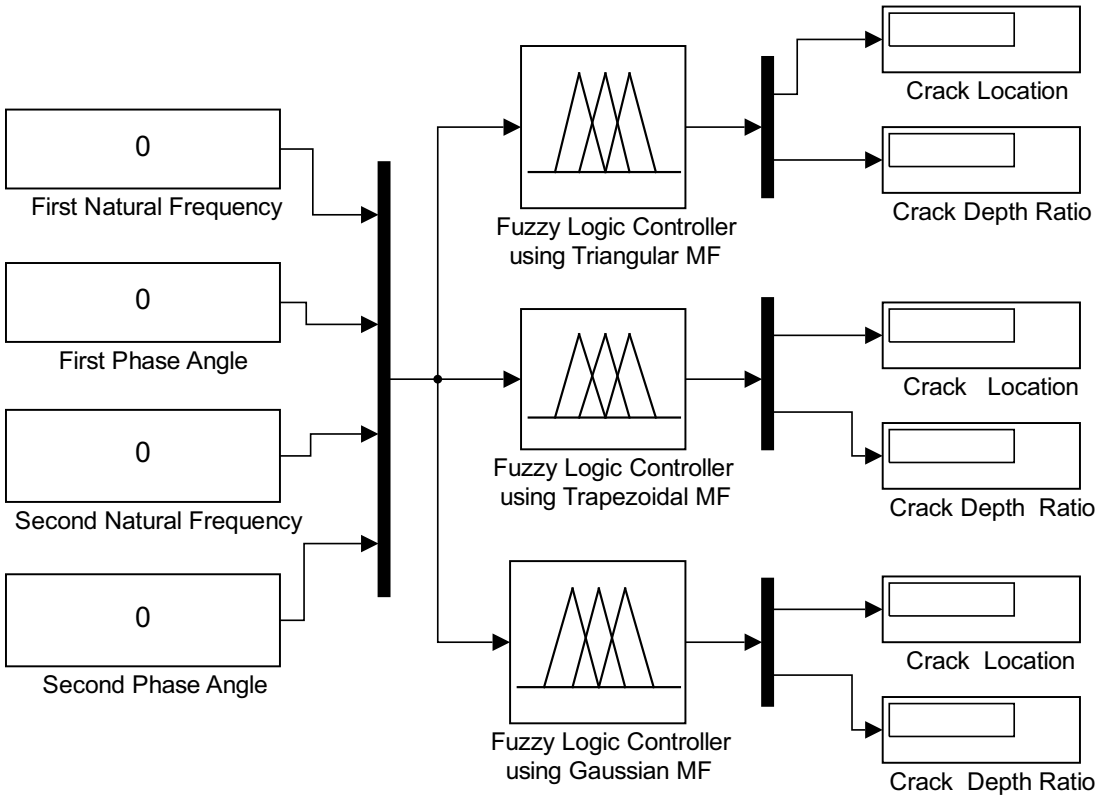

Figure 5.4: Simulink model for identification of crack

Chapter 6

Results and Discussions

6.1 Introduction

The problem definition, objective, and significance of the thesis work have been described in chapter one. In this work, the strategy used for detecting crack is identifying crack signature parameters using different theoretical analysis tools. An analytical model for both cracked and uncracked shafts is developed using finite element analysis. The mathematical model is programmed in Matlab for the determination of crack signature parameters. Also, corresponding shafts with the same dimension are modelled in Solidwork and simulated in Ansys for the same purpose. So, in this chapter, various crack locations and crack depths are taken to notice the change in the first two natural frequencies.

Using different types of membership functions, such as triangular, trapezoidal, and Gaussian, a fuzzy inference system has been built for the identification of cracks (crack depth and crack location). The developed fuzzy inference system uses first natural frequency, second natural frequency, first phase angle, and second phase angle as inputs and the crack depth and the crack location as output. For the design of a fuzzy inference system, several linguistic terms and fuzzy rules have been developed. The analysis of the results is described below.

6.2 Correlation Coefficient and Average Total Error

The degree and direction for the relation between two variables are called correlation. The correlation coefficient is the quantification or the measure of the degree of association between statistical variables, mathematical variables, phenomena, or between different things. It's denoted by 'r' and mostly quantified with a number between -1 and +1. But, the interpretation of these numbers is significantly different among scientific research areas [93, 94].

In this work, the correlation coefficient is used to know the closeness between results from Ansys and Matlab. Also, it is used to verify the outputs from the triangular, trapezoidal, and Gaussian membership functions with the theoretical proposed values. So using Taylor [93] and Schober et al. [95] Interpretations as a guide, in this study, the 0 value shows there is no closeness between the results of software's or between different fuzzy membership functions and theoretical proposed values. The value 1 shows there is a strong or perfect closeness between the results of software or between different fuzzy membership functions and theoretical proposed values. This implies as the correlation coefficient increases from 0 to +1 the strength of values closeness is increased.

The average total error is the method of determining the closeness of values between different parameters. In this study, this method is used for a similar purpose to the correlation coefficient. The equations for the mathematical determination of the correlation coefficient and the average total error are described in Appendix B.

6.3 Comparison of Matlab and Ansys Results

For numerical analysis, the turbine shaft and corresponding impeller (disc) were dimensioned similarly for both analysis tools. Also, their operational condition is uniform. Ansys is used as a reference to verify the Matlab results that were developed from theoretical equations. Consider there is a crack in a shaft at a length of 208.6 mm (from left bearing) with a dimensionless depth ratio of 0.5. The crack is formed at a specified location of the shaft with specified depths in Solidwork premium. Then modal analysis

has been performed in Ansys by importing the IGES file. In the same way, the differential equation of the cracked shaft has been simulated at the specified location and depth of crack in Matlab. Figures 6.1 to 6.4 show the modal results from Matlab and Ansys. The first mode natural frequency value from Matlab is 17.9733 Hz (see Figure 6.1) and 17.798 Hz (see Figure 6.2) from Ansys. Also as depicted in Figures 6.3 and 6.4, the second mode natural frequency value from Matlab and Ansys are 30.2226 Hz and 32.558 Hz respectively.

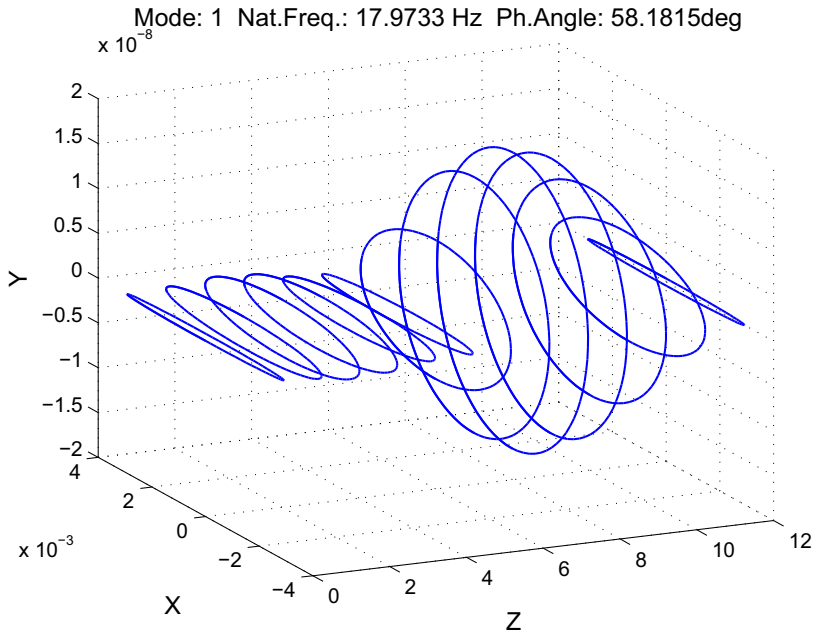

Figure 6.1: First mode results from Matlab modal analysis

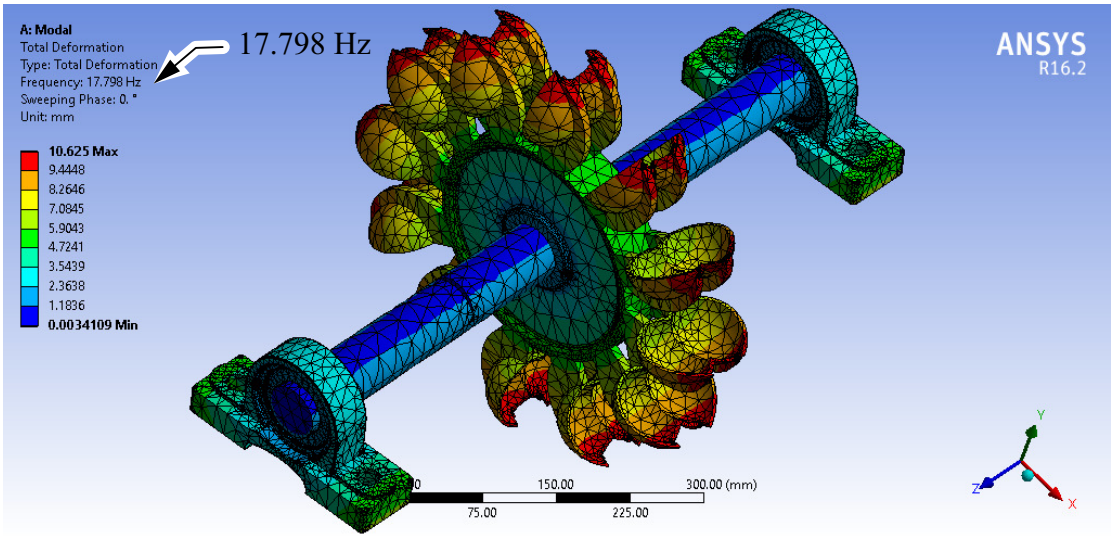

Figure 6.2: First mode results from Ansys modal analysis

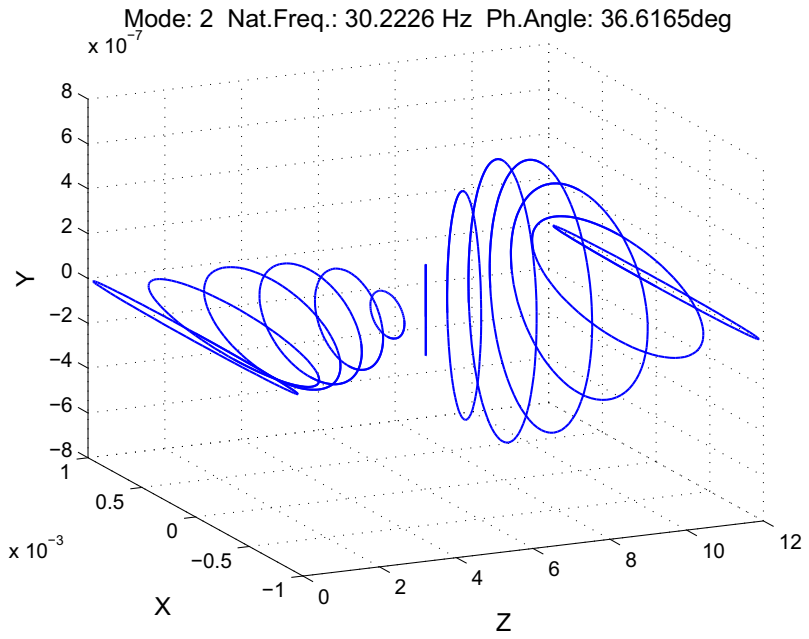

Figure 6.3: Second mode results from Matlab modal analysis

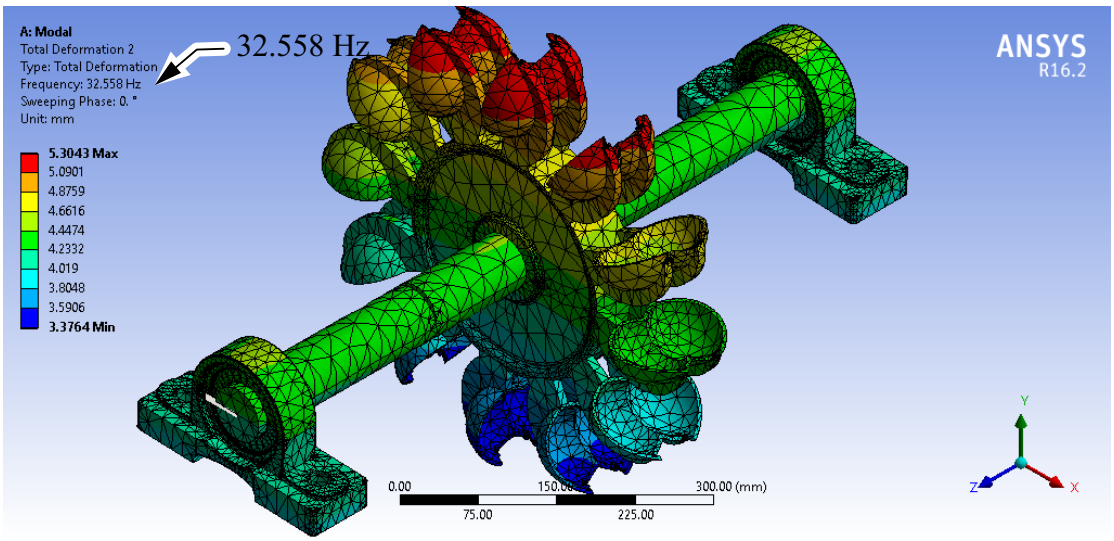

Figure 6.4: Second mode results from Ansys modal analysis

This shows that at the same location and same depth ratio of crack, the Matlab and Ansys modal results are close to each other. Table 6.1 below shows the comparison between Ansys and Matlab modal analysis results for different depths of crack at different locations.

Table 6.1: Comparison of Ansys and Matlab modal analyses for mode one

Crack location (mm)	Crack depth ratio	First mode Ansys	First mode Matlab	Second mode Ansys	Second mode Matlab
89.4	0.1	18.766	18.0294	32.831	30.2252
	0.25	18.251	18.0291	32.815	30.2251
	0.5	18.101	18.0273	32.796	30.2248
208.6	0.1	18.421	17.9831	32.698	30.2233
	0.25	18.202	17.9816	32.681	30.2232
	0.5	17.789	17.9733	32.558	30.2226
268.2	0.1	18.268	17.9515	32.713	30.2238
	0.25	18.065	17.9493	32.691	30.2237
	0.5	17.017	17.9365	32.686	30.2232
327.8	0.1	18.005	17.9167	32.836	30.2247
	0.25	17.672	17.9137	32.817	30.2246
	0.5	16.997	17.896	32.786	30.2242
Correlation coefficient factor		***0.706***		***0.965***	
Average total error (%)		***2.091***		***7.737***	

When the results obtained from the analysis of the cracked turbine shaft in Matlab are compared with the results from the Ansys, the correlation coefficients were found to be within 0.706 for the first mode and 0.965 for the second mode. These values are above zero and almost have much closer to one, which indicates good agreement between results. Also, the average total errors between the two software's are 2.091% and 7.737% for mode one and mode two respectively. Since the average total errors are below 10%, the results from Ansys and Matlab are close to each other. So for crack identification, results obtained from both modes are used as inputs for the fuzzy controller.

6.4 Results of Fuzzy Logic Method for Crack Identification

Crack signature parameters (first natural frequency, first phase angle, second natural frequency, and second phase angle) obtained from previous theoretical analysis tools are great indicators for the presence of a crack. Determining these parameters is the forward method. On the other hand, identifying the location and depth of the crack using these parameters is called the backward method. So these parameters are inputs for the fuzzy inference system. In response, crack location and crack depth are output parameters. So, the first two modal results are trained for crack identification in the fuzzy logic algorithm.

In section 6.3 above, the crack signature parameters are determined at the crack location of 208.6 mm and a dimensionless depth ratio of 0.5. The first and second modes natural frequencies of the shaft were 17.9733 Hz and 30.2226 Hz respectively. Also, the corresponding first and second mode phase angles of the shaft were 58.1815 degrees and 36.6165 degrees respectively. So this section intends to identify the location and depth of the crack using these results as input to the fuzzy controller. As illustrated in Figure 6.5, the Simulink model from the three different membership functions forecasts the location and depth ratio of crack around 209 mm and 0.5 respectively. This indicates that the fuzzy controller predicts the location and depth of the crack almost accurately.

6.4.1 Comparison of theoretical and fuzzy logic results

Tables 1, 2 and 3 in Appendix C shows the comparison of the results obtained from theoretical and fuzzy controllers using triangle, trapezoidal, and Gaussian membership functions. By the consideration of the triangular membership function, the correlation coefficients are 0.9993 for identifying both crack location and crack depth. When applying the trapezoidal membership function, the correlation coefficients in detecting crack location and crack depth are 0.999 and 0.9878 respectively. Similarly, the correlation coefficients for identifying the crack location and determining the crack depth using the Gaussian membership function are 0.9998 and 0.9997, respectively. Since these numbers are so close to one, it means that the FL results and the theoretical

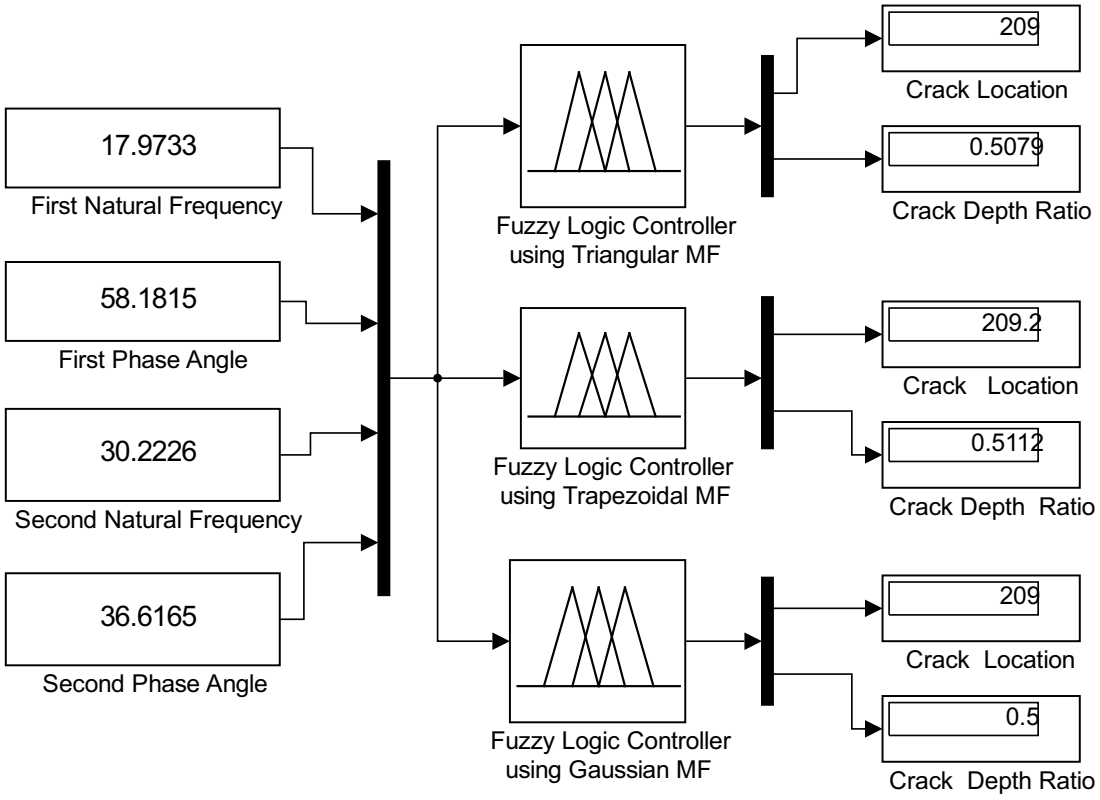

Figure 6.5: Result from Simulink model

crack locations and depths are in very good agreement.

Similarly as depicted in Table 1 of Appendix C, by the consideration of the triangular membership function, the average total error for detecting crack location is 0.31%, and crack depth is 0.78%. When applying the trapezoidal membership function, the average total errors for detecting crack location and crack depth are 0.34% and 4.82% respectively (illustrated in Table 2 of Appendix C). In the same way, the average total errors for identifying the crack location and determining the crack depth using the Gaussian membership function are 0.29% and 0.58%, respectively (see Table 3 of Appendix C). From these results, the average total errors of all membership functions are very small. Therefore, it is possible to use all these membership functions for the identification of cracks.

However, when compared to the other two membership functions, the average total errors of the Gaussian membership function are lower. Also, as compared to other membership functions, the values of the correlation coefficient in the Gaussian membership

function are significantly closer to one. As a result, the Gaussian membership function is preferred over the triangular and trapezoidal membership functions in this study.

6.4.2 Characteristic curves

The following different characteristic curves show the closeness of the outputs from the fuzzy controller membership functions with the theoretical values. Figures 6.6, 6.7, and 6.8 are for crack depth ratio and Figures 6.9 and 6.10 are for crack location. All characteristic curves show that results from the three membership functions have good agreement with the theoretical values. Even though the results of the three membership functions are close to the theoretical values, the Gaussian membership function has the best agreement.

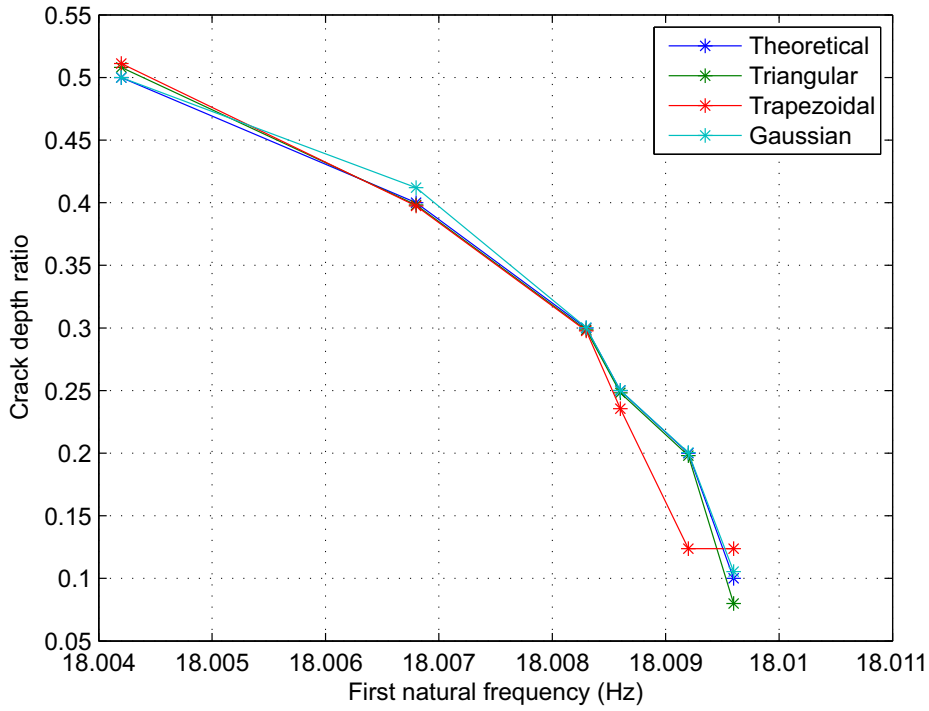

Figure 6.6: Characteristic curve for first mode natural frequency versus crack depth ratio

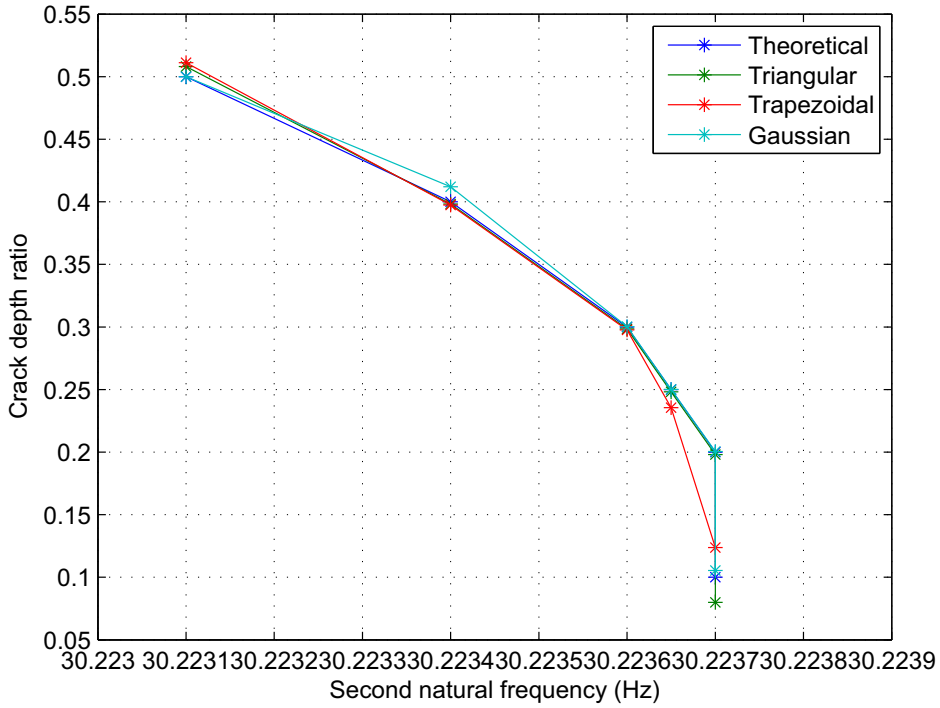

Figure 6.7: Characteristic curve for second mode natural frequency versus crack depth ratio

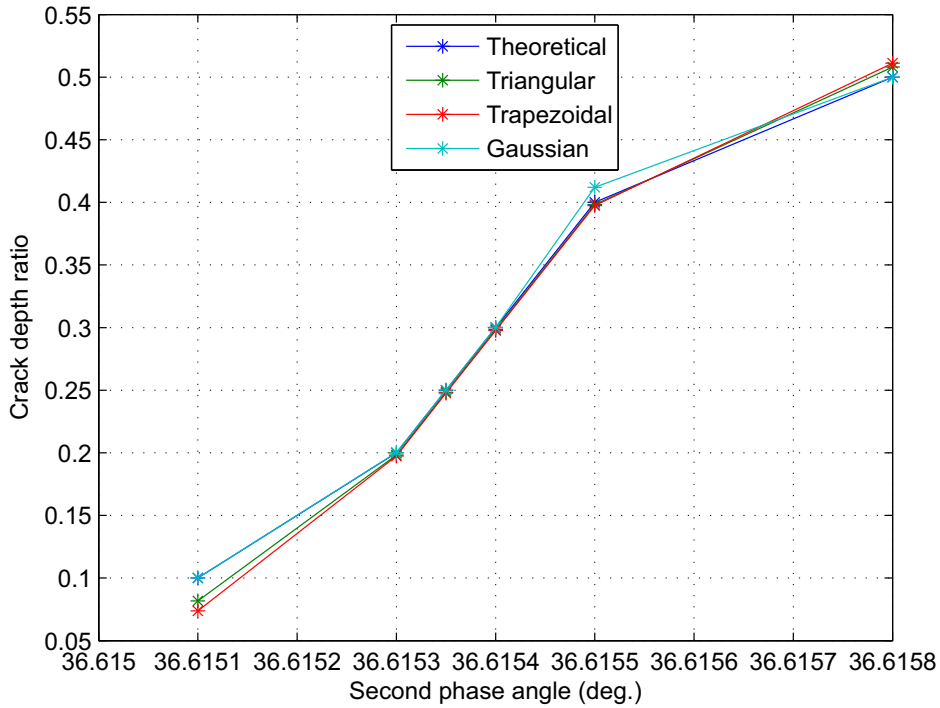

Figure 6.8: Characteristic curve for second mode phase angle versus crack depth ratio

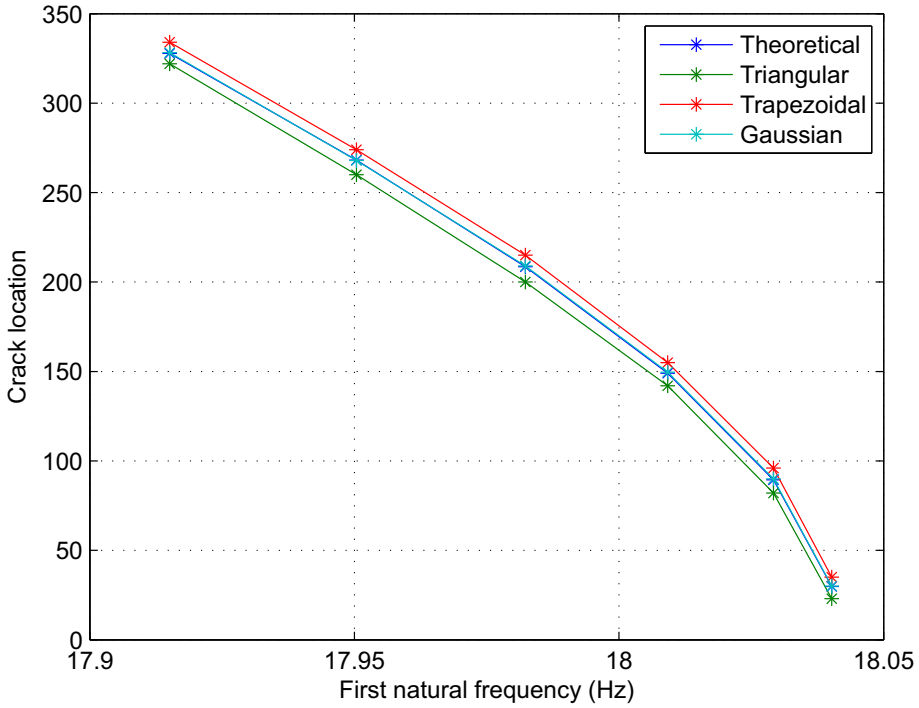

Figure 6.9: Characteristic curve for first mode natural frequency versus crack location

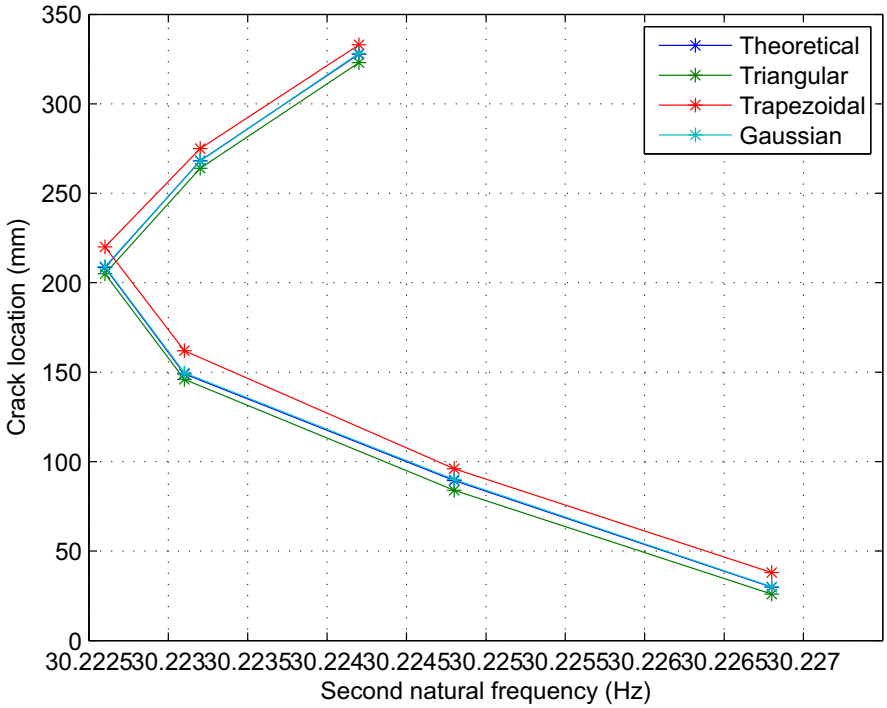

Figure 6.10: Characteristic curve for second mode natural frequency versus crack location

6.5 Applications

i. Because the fuzzy logic method of crack identification is non-destructive in nature, it can be employed efficiently for online condition monitoring of engineering systems.

ii. The crack detection algorithm developed can be used to forecast cracks in hydroelectric generations, turbo equipment, nuclear plants and ship structures, as well as biomedical engineering systems, and other areas.

Chapter 7

Conclusion and Recommendations

7.1 Conclusion

This thesis discusses the impact of transverse cracks on a vibrating uniform circular shaft. The main purpose of this study has been to come up with a quick and efficient method for detecting cracks in vibrating structures. The vibration analysis has been carried out using theoretical and intelligent methodology using fuzzy logic. Natural frequency and phase angle were used to identify cracks in this investigation, and the crack depth and crack location were determined. The following findings are drawn from the results of the analyses performed on the cracked shaft.

i. The presence of a transverse crack was investigated, and it was discovered that the presence of the crack has an impact on the natural frequency and phase angle of the shaft. As crack depth increases, the natural frequency decreases, and the corresponding phase angle increases. As a result, it is concluded that the analysis of natural frequency and phase angle change is effective for crack prediction in shafts.

ii. The crack depth and crack location were determined by comparing the vibration analysis results of the uncracked and cracked shafts.

iii. For the investigation of crack detection, a fuzzy inference system was constructed utilizing different membership functions, and it was discovered that the fuzzy controller predicts the crack depth and crack location as close to the theoretical analysis results. The fuzzy inference system's most important feature is that it predicts results with less computational time.

iv. The training data for the fuzzy inference system are the first two natural frequencies and their corresponding phase angles obtained from the theoretical study. The results of the theoretical and fuzzy logic analysis are in good agreement.

7.2 Recommendation and Future work

i. The fuzzy inference system's analysis can be extended for localization and identification of multiple cracks in turbine-generator shaft lines.

ii. The change in vibration characteristics will be studied by the consideration of shaft misalignment and bearing tilt.

iii. The current research work's entire analysis is based on an Euler Bernoulli beam-like structure, which can be extended to include a Timoshenko beam-like structure.

iv. Fuzzy logic and other artificial intelligence approaches can be hybridized to provide a new method for detecting cracks in turbine shafts.

References

[1] A. Heng, S. Zhang, A. Tan, and J. Mathew, "Rotating machinery prognostics: State of the art, challenges and opportunities," *Mechanical systems and signal processing*, vol. 23, no. 3, pp. 724–739, 2009.

[2] M. Vishwakarma, R. Purohit, V. Harshlata, and P. Rajput, "Vibration analysis& condition monitoring for rotating machines: a review," *Materials Today: Proceedings*, vol. 4, no. 2, pp. 2659–2664, 2017.

[3] P. Zhang and D. Lu, "A survey of condition monitoring and fault diagnosis toward integrated o&m for wind turbines," *Energies*, vol. 12, no. 14, p. 2801, 2019.

[4] C. Nath, "Integrated tool condition monitoring systems and their applications: a comprehensive review," *Procedia Manufacturing*, vol. 48, pp. 852–863, 2020.

[5] A. Oberholster and S. Heyns, "On-line fan blade damage detection using neural networks," *Mechanical systems and signal processing*, vol. 20, no. 1, pp. 78–93, 2006.

[6] J. Sinou and A. Lees, "The influence of cracks in rotating shafts," *Journal of sound and vibration*, vol. 285, no. 4-5, pp. 1015–1037, 2005.

[7] H. Towsyfyan, A. Biguri, R. Boardman, and T. Blumensath, "Successes and challenges in non-destructive testing of aircraft composite structures," *Chinese Journal of Aeronautics*, vol. 33, no. 3, pp. 771–791, 2020.

[8] M. Dong and J. Chen, "Crack identification in a rotor with an open crack," *Journal of mechanical science and technology*, vol. 23, no. 11, pp. 2964–2972, 2009.

[9] N. Bachschmid, P. Pennacchi, and A. Vania, "Diagnostic significance of orbit shape analysis and its application to improve machine fault detection," *Journal of*

the Brazilian Society of Mechanical Sciences and Engineering, vol. 26, pp. 200–208, 2004.

[10] S. Prasad and A. Sekhar, "Detection and localization of fatigue-induced transverse crack in a rotor shaft using principal component analysis," *Structural Health Monitoring*, vol. 20, no. 2, pp. 513–531, 2021.

[11] A. Sekhar, "Identification of a crack in a rotor system using a model-based wavelet approach," *Structural Health Monitoring*, vol. 2, no. 4, pp. 293–308, 2003.

[12] Y. Wang, X. Xiong, and X. Hu, "Vibration and stability analysis of a bearing rotor system with transverse breathing crack and initial bending," *Machines*, vol. 9, no. 4, p. 79, 2021.

[13] T. Liong and C. Proppe, "Application of the cohesive zone model for the evaluation of stiffness losses in a rotor with a transverse breathing crack," *Journal of Sound and Vibration*, vol. 332, no. 8, pp. 2098–2110, 2013.

[14] M. Cerri, M. Dilena, and G. Ruta, "Vibration and damage detection in undamaged and cracked circular arches: experimental and analytical results," *Journal of sound and vibration*, vol. 314, no. 1-2, pp. 83–94, 2008.

[15] I. Mahfouz and A. Banerjee, "Crack detection and identification using vibration signals and fuzzy clustering," *Procedia Computer Science*, vol. 114, pp. 266–274, 2017.

[16] E. Douka and L. Hadjileontiadis, "Time–frequency analysis of the free vibration response of a beam with a breathing crack," *Ndt & E International*, vol. 38, no. 1, pp. 3–10, 2005.

[17] H. Mongy and Y. Younes, "Vibration analysis of a multi-fault transient rotor passing through sub-critical resonances," *Journal of Vibration and Control*, vol. 24, no. 14, pp. 2986–3009, 2018.

[18] A. Bovsunovsky and V. Matveev, "Analytical approach to the determination of dynamic characteristics of a beam with a closing crack," *Journal of sound and vibration*, vol. 235, no. 3, pp. 415–434, 2000.

[19] Q. Han, J. Zhao, and F. Chu, "Dynamic analysis of a geared rotor system considering a slant crack on the shaft," *Journal of Sound and Vibration*, vol. 331, no. 26, pp. 5803–5823, 2012.

[20] A. Hossain, L. Humphrey, and A. Mian, "Prediction of the dynamic response of a mini-cantilever beam partially submerged in viscous media using finite element method," *Finite elements in analysis and design*, vol. 48, no. 1, pp. 1339–1345, 2012.

[21] D. Gayen, R. Tiwari, and D. Chakraborty, "Finite element based stability analysis of a rotor-bearing system having a functionally graded shaft with transverse breathing cracks," *International Journal of Mechanical Sciences*, vol. 157, pp. 403–414, 2019.

[22] A. Sekhar, "Vibration characteristics of a cracked rotor with two open cracks," *Journal of Sound and Vibration*, vol. 223, no. 4, pp. 497–512, 1999.

[23] M. Silani, S. Rad, and H. Talebi, "Vibration analysis of rotating systems with open and breathing cracks," *Applied Mathematical Modelling*, vol. 37, no. 24, pp. 9907–9921, 2013.

[24] Z. Lu, Y. Lv, and H. Ouyang, "A super-harmonic feature based updating method for crack identification in rotors using a kriging surrogate model," *Applied Sciences*, vol. 9, no. 12, p. 2428, 2019.

[25] M. Abdo and M. Hori, "A numerical study of structural damage detection using changes in the rotation of mode shapes," *Journal of Sound and vibration*, vol. 251, no. 2, pp. 227–239, 2002.

[26] K. Song, C. Noh, and C. Choi, "A new three-dimensional finite element analysis model of high-speed train–bridge interactions," *Engineering Structures*, vol. 25, no. 13, pp. 1611–1626, 2003.

[27] J. Kim and N. Stubbs, "Improved damage identification method based on modal information," *Journal of Sound and Vibration*, vol. 252, no. 2, pp. 223–238, 2002.

[28] T. Chondros, A. Dimarogonas, and J. Yao, "A continuous cracked beam vibration theory," *Journal of sound and vibration*, vol. 215, no. 1, pp. 17–34, 1998.

[29] R. Fotouhi, "Dynamic analysis of very flexible beams," *Journal of Sound and Vibration*, vol. 305, no. 3, pp. 521–533, 2007.

[30] T. Quek, Q. Wang, L. Zhang, and K. Ang, "Sensitivity analysis of crack detection in beams by wavelet technique," *International journal of mechanical sciences*, vol. 43, no. 12, pp. 2899–2910, 2001.

[31] B. Yang, C. Suh, and A. Chan, "Characterization and detection of crack-induced rotary instability," *J. Vib. Acoust.*, vol. 124, no. 1, pp. 40–48, 2002.

[32] S. Loutridis, E. Douka, and A. Trochidis, "Crack identification in double-cracked beams using wavelet analysis," *Journal of sound and vibration*, vol. 277, no. 4-5, pp. 1025–1039, 2004.

[33] J. Xiang, X. Chen, Q. Mo, and Z. He, "Identification of crack in a rotor system based on wavelet finite element method," *Finite Elements in Analysis and Design*, vol. 43, no. 14, pp. 1068–1081, 2007.

[34] G. Qian, S. Gu, and J. Jiang, "The dynamic behaviour and crack detection of a beam with a crack," *Journal of sound and vibration*, vol. 138, no. 2, pp. 233–243, 1990.

[35] J. Ma, J. Xue, S. Yang, and Z. He, "A study of the construction and application of a daubechies wavelet-based beam element," *Finite Elements in Analysis and Design*, vol. 39, no. 10, pp. 965–975, 2003.

[36] A. Gentile and A. Messina, "On the continuous wavelet transforms applied to discrete vibrational data for detecting open cracks in damaged beams," *International Journal of Solids and Structures*, vol. 40, no. 2, pp. 295–315, 2003.

[37] B. Li, X. Chen, J. Ma, and Z. He, "Detection of crack location and size in structures using wavelet finite element methods," *Journal of Sound and Vibration*, vol. 285, no. 4-5, pp. 767–782, 2005.

[38] R. Sino, T. Baranger, E. Chatelet, and G. Jacquet, "Dynamic analysis of a rotating composite shaft," *Composites Science and Technology*, vol. 68, no. 2, pp. 337–345, 2008.

[39] C. Stoisser and S. Audebert, "A comprehensive theoretical, numerical and experimental approach for crack detection in power plant rotating machinery," *Mechanical systems and signal processing*, vol. 22, no. 4, pp. 818–844, 2008.

[40] M. Gómez, C. Castejón, and J. Prada, "Crack detection in rotating shafts based on 3× energy: Analytical and experimental analyses," *Mechanism and Machine Theory*, vol. 96, pp. 94–106, 2016.

[41] N. Shulzhenko and G. Ovcharova, "Effect of break of the elastic axis of a rotor with transverse crack on its vibrational characteristics," *Strength of materials*, vol. 29, no. 4, pp. 380–385, 1997.

[42] J. Wang, D. Qin, and T. Lim, "Dynamic analysis of horizontal axis wind turbine by thin-walled beam theory," *Journal of Sound and Vibration*, vol. 329, no. 17, pp. 3565–3586, 2010.

[43] H. Dong, X. Chen, B. Li, K. Qi, and Z. He, "Rotor crack detection based on high-precision modal parameter identification method and wavelet finite element model," *Mechanical Systems and Signal Processing*, vol. 23, no. 3, pp. 869–883, 2009.

[44] A. Presas, D. Valentin, C. Valero, M. Egusquiza, and E. Egusquiza, "Experimental measurements of the natural frequencies and mode shapes of rotating disk-blades-disk assemblies from the stationary frame," *Applied Sciences*, vol. 9, no. 18, p. 3864, 2019.

[45] J. Chou and J. Ghaboussi, "Genetic algorithm in structural damage detection," *Computers & structures*, vol. 79, no. 14, pp. 1335–1353, 2001.

[46] M. Vakil, M. Peimani, M. Sadeghi, and M. Ettefagh, "Crack detection in beam-like structures using genetic algorithms," *Applied soft computing*, vol. 8, no. 2, pp. 1150–1160, 2008.

[47] E. Shopova and N. Vaklieva, "Basic—a genetic algorithm for engineering problems solution," *Computers & chemical engineering*, vol. 30, no. 8, pp. 1293–1309, 2006.

[48] M. Mungla, D. Sharma, and R. Trivedi, "Identification of a crack in clamped-clamped beam using frequency-based method and genetic algorithm," *Procedia Engineering*, vol. 144, pp. 1426–1434, 2016.

[49] P. Pawar and R. Ganguli, "Genetic fuzzy system for online structural health monitoring of composite helicopter rotor blades," *Mechanical Systems and Signal Processing*, vol. 21, no. 5, pp. 2212–2236, 2007.

[50] T. Boutros and M. Liang, "Mechanical fault detection using fuzzy index fusion," *International Journal of Machine Tools and Manufacture*, vol. 47, no. 11, pp. 1702–1714, 2007.

[51] M. Chandrashekhar and R. Ganguli, "Damage assessment of structures with uncertainty by using mode-shape curvatures and fuzzy logic," *Journal of Sound and Vibration*, vol. 326, no. 3-5, pp. 939–957, 2009.

[52] L. Miguel and F. Blázquez, "Fuzzy logic-based decision-making for fault diagnosis in a dc motor," *Engineering Applications of Artificial Intelligence*, vol. 18, no. 4, pp. 423–450, 2005.

[53] V. Sugumaran and K. Ramachandran, "Fault diagnosis of roller bearing using fuzzy classifier and histogram features with focus on automatic rule learning," *Expert Systems with Applications*, vol. 38, no. 5, pp. 4901–4907, 2011.

[54] C. Kao and L. Hung, "Detection of structural damage via free vibration responses generated by approximating artificial neural networks," *Computers & Structures*, vol. 81, no. 28-29, pp. 2631–2644, 2003.

[55] A. Mohammed, R. Neilson, W. Deans, and P. MacConnell, "Crack detection in a rotating shaft using artificial neural networks and psd characterisation," *Meccanica*, vol. 49, no. 2, pp. 255–266, 2014.

[56] Q. Chen, Y. Chan, and K. Worden, "Structural fault diagnosis and isolation using neural networks based on response-only data," *Computers & Structures*, vol. 81, no. 22-23, pp. 2165–2172, 2003.

[57] N. Saravanan, K. Siddabattuni, and K. Ramachandran, "Fault diagnosis of spur bevel gear box using artificial neural network (ann), and proximal support vector machine (psvm)," *Applied soft computing*, vol. 10, no. 1, pp. 344–360, 2010.

[58] W. Zhao, C. Hua, D. Dong, and H. Ouyang, "A novel method for identifying crack and shaft misalignment faults in rotor systems under noisy environments based on cnn," *Sensors*, vol. 19, no. 23, p. 5158, 2019.

[59] W. Liu, J. Huang, C. Sung, and C. Lee, "Detection of cracks using neural networks and computational mechanics," *Computer methods in applied mechanics and engineering*, vol. 191, no. 25-26, pp. 2831–2845, 2002.

[60] M. Mehrjoo, N. Khaji, H. Moharrami, and A. Bahreininejad, "Damage detection of truss bridge joints using artificial neural networks," *Expert systems with applications*, vol. 35, no. 3, pp. 1122–1131, 2008.

[61] A. Quteishat and P. Lim, "A modified fuzzy min–max neural network with rule extraction and its application to fault detection and classification," *Applied Soft Computing*, vol. 8, no. 2, pp. 985–995, 2008.

[62] B. Samanta, "Gear fault detection using artificial neural networks and support vector machines with genetic algorithms," *Mechanical systems and signal processing*, vol. 18, no. 3, pp. 625–644, 2004.

[63] H. Firpi and G. Vachtsevanos, "Genetically programmed-based artificial features extraction applied to fault detection," *Engineering Applications of Artificial Intelligence*, vol. 21, no. 4, pp. 558–568, 2008.

[64] D. Agarwalla, S. Khan, and K. Sahoo, "Application of genetic fuzzy system for damage identification in cantilever beam structure," *Procedia engineering*, vol. 144, pp. 215–225, 2016.

[65] M. Friswell, J. Penny, S. Garvey, and A. Lees, *Dynamics of rotating machines*. Cambridge university press, 2010.

[66] H. Nelson and J. McVaugh, "The dynamics of rotor-bearing systems using finite elements," *Journal of Engineering for Industry*, no. 75, pp. 593–600, 1976.

[67] A. Nassis, "Analyses of a rotor dynamic testrigs," Master's thesis, Luleå University of Technology, Sweden, 2010.

[68] N. Ganesan and R. Engels, "Hierarchical bernoulli-euler beam finite elements," *Computers & structures*, vol. 43, no. 2, pp. 297–304, 1992.

[69] H. Nelson, "A finite rotating shaft element using timoshenko beam theory," *Journal of Mechanical Design*, vol. 102, pp. 793–803, 1980.

[70] M. Shudeifat and E. Butcher, "On the modeling of open and breathing cracks of a cracked rotor system," in *International Design Engineering Technical Conferences and Computers and Information in Engineering Conference*, vol. 44137, pp. 919–928, 2010.

[71] M. Shudeifat and E. Butcher, "New breathing functions for the transverse breathing crack of the cracked rotor system: approach for critical and subcritical harmonic analysis," *Journal of Sound and Vibration*, vol. 330, no. 3, pp. 526–544, 2011.

[72] M. Shudeifat, "On the finite element modeling of the asymmetric cracked rotor," *Journal of sound and vibration*, vol. 332, no. 11, pp. 2795–2807, 2013.

[73] W. Pilkey, *Analysis and design of elastic beams: Computational methods*. John Wiley & Sons, 2002.

[74] H. Hwang and C. Kim, "Damage detection in structures using a few frequency response measurements," *Journal of sound and vibration*, vol. 270, no. 1-2, pp. 1–14, 2004.

[75] V. Ganguly and T. Schmitz, "Phase correction for frequency response function measurements," *Precision Engineering*, vol. 38, no. 2, pp. 409–413, 2014.

[76] B. Kirchgäßner, "Finite elements in rotordynamics," *Procedia Engineering*, vol. 144, pp. 736–750, 2016.

[77] S. Čorović and D. Miljavec, "Modal analysis and rotor-dynamics of an interior permanent magnet synchronous motor: An experimental and theoretical study," *Applied Sciences*, vol. 10, no. 17, p. 5881, 2020.

[78] L. Zadeh, "Fuzzy logic—a personal perspective," *Fuzzy sets and systems*, vol. 281, pp. 4–20, 2015.

[79] L. Zadeh, "Toward a perception-based theory of probabilistic reasoning with imprecise probabilities," *Journal of Statistical Planning and Inference*, vol. 105, pp. 233–264, 2002.

[80] E. Mamdani and S. Assilian, "An experiment in linguistic synthesis with a fuzzy logic controller," *International journal of man-machine studies*, vol. 7, no. 1, pp. 1–13, 1975.

[81] W. Yu and X. Li, "Online fuzzy modeling with structure and parameter learning," *Expert Systems with Applications*, vol. 36, no. 4, pp. 7484–7492, 2009.

[82] M. Azeem, N. Ahmad, and M. Hanmandlu, "Fuzzy modeling of fluidized catalytic cracking unit," *Applied Soft Computing*, vol. 7, no. 1, pp. 298–324, 2007.

[83] T. Abdelazim and O. Malik, "Identification of nonlinear systems by takagi–sugeno fuzzy logic grey box modeling for real-time control," *Control Engineering Practice*, vol. 13, no. 12, pp. 1489–1498, 2005.

[84] A. Trabelsi, F. Lafont, M. Kamoun, and G. Enea, "Fuzzy identification of a greenhouse," *Applied Soft Computing*, vol. 7, no. 3, pp. 1092–1101, 2007.

[85] H. Suzuki, "Fuzzy sets and membership functions," *Fuzzy sets and systems*, vol. 58, no. 2, pp. 123–132, 1993.

[86] S. Medasani, J. Kim, and R. Krishnapuram, "An overview of membership function generation techniques for pattern recognition," *International Journal of approximate reasoning*, vol. 19, no. 3-4, pp. 391–417, 1998.

[87] A. Ajofoyinbo, V. Olunloyo, O. Obe, *et al.*, "On development of fuzzy controller: The case of gaussian and triangular membership functions," *Journal of Signal and Information Processing*, vol. 2, no. 04, p. 257, 2011.

[88] L. Zadeh, "The concept of a linguistic variable and its application to approximate reasoning—i," *Information sciences*, vol. 8, no. 3, pp. 199–249, 1975.

[89] V. Talekar, V. Bhanuse, and J. Kulkarni, "Vibration analysis of cracked beam using fuzzy logic technique," in *2016 International Conference on Automatic Control and Dynamic Optimization Techniques (ICACDOT)*, pp. 678–682, IEEE, 2016.

[90] X. Fang, H. Luo, and J. Tang, "Structural damage detection using neural network with learning rate improvement," *Computers & structures*, vol. 83, no. 25-26, pp. 2150–2161, 2005.

[91] Y. Kim, S. Ahn, and W. Kwon, "Computational complexity of general fuzzy logic control and its simplification for a loop controller," *Fuzzy Sets and Systems*, vol. 111, no. 2, pp. 215–224, 2000.

[92] H. Das and D. Parhi, "Online fuzzy logic crack detection of a cantilever beam," *International Journal of Knowledge-based and Intelligent Engineering Systems*, vol. 12, no. 2, pp. 157–171, 2008.

[93] R. Taylor, "Interpretation of the correlation coefficient: a basic review," *Journal of diagnostic medical sonography*, vol. 6, no. 1, pp. 35–39, 1990.

[94] L. Goodwin and N. Leech, "Understanding correlation: Factors that affect the size of r," *The Journal of Experimental Education*, vol. 74, no. 3, pp. 249–266, 2006.

[95] P. Schober, C. Boer, and L. Schwarte, "Correlation coefficients: appropriate use and interpretation," *Anesthesia & Analgesia*, vol. 126, no. 5, pp. 1763–1768, 2018.

Appendix

Appendix A

Some fuzzy rules for fuzzy inference system

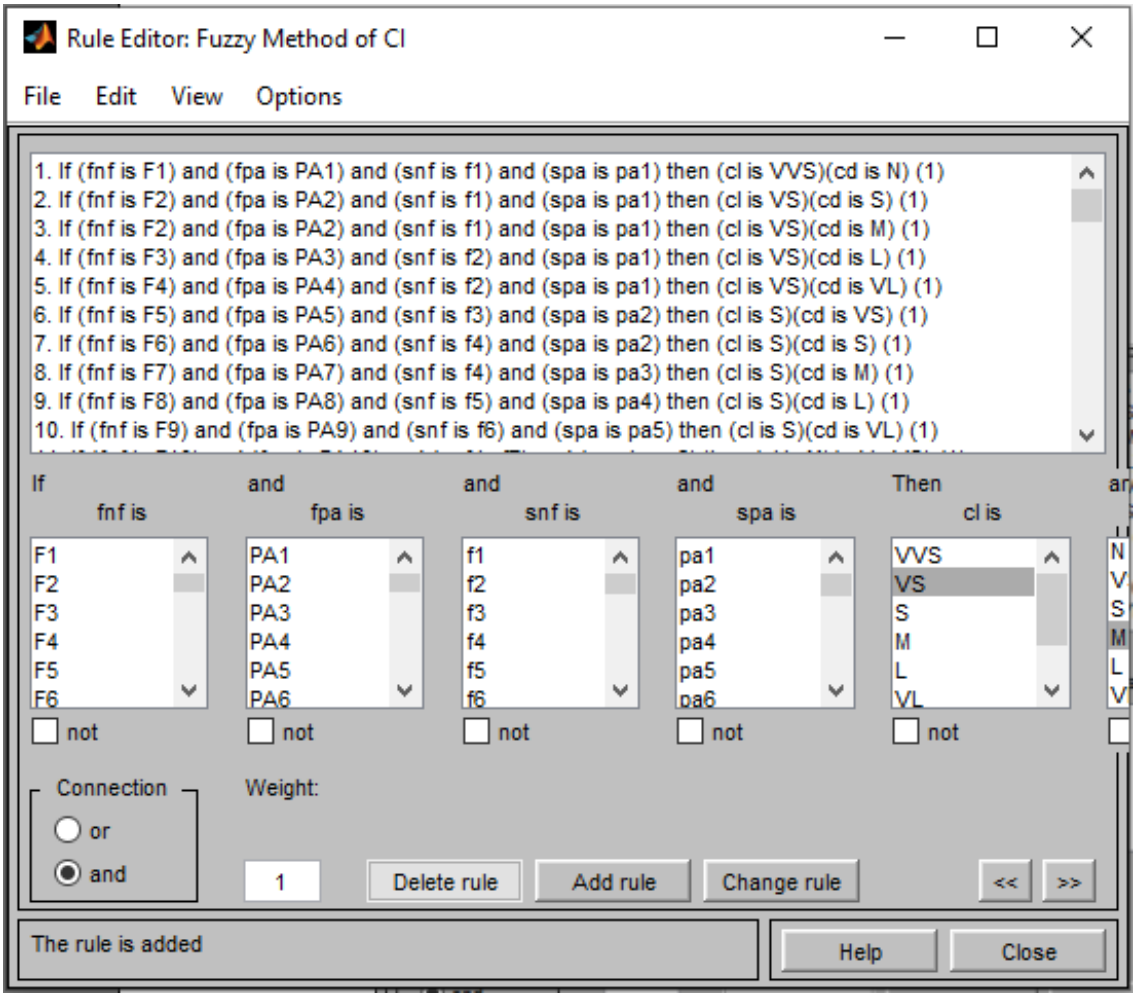

Figure 1: Fuzzy Logic rules

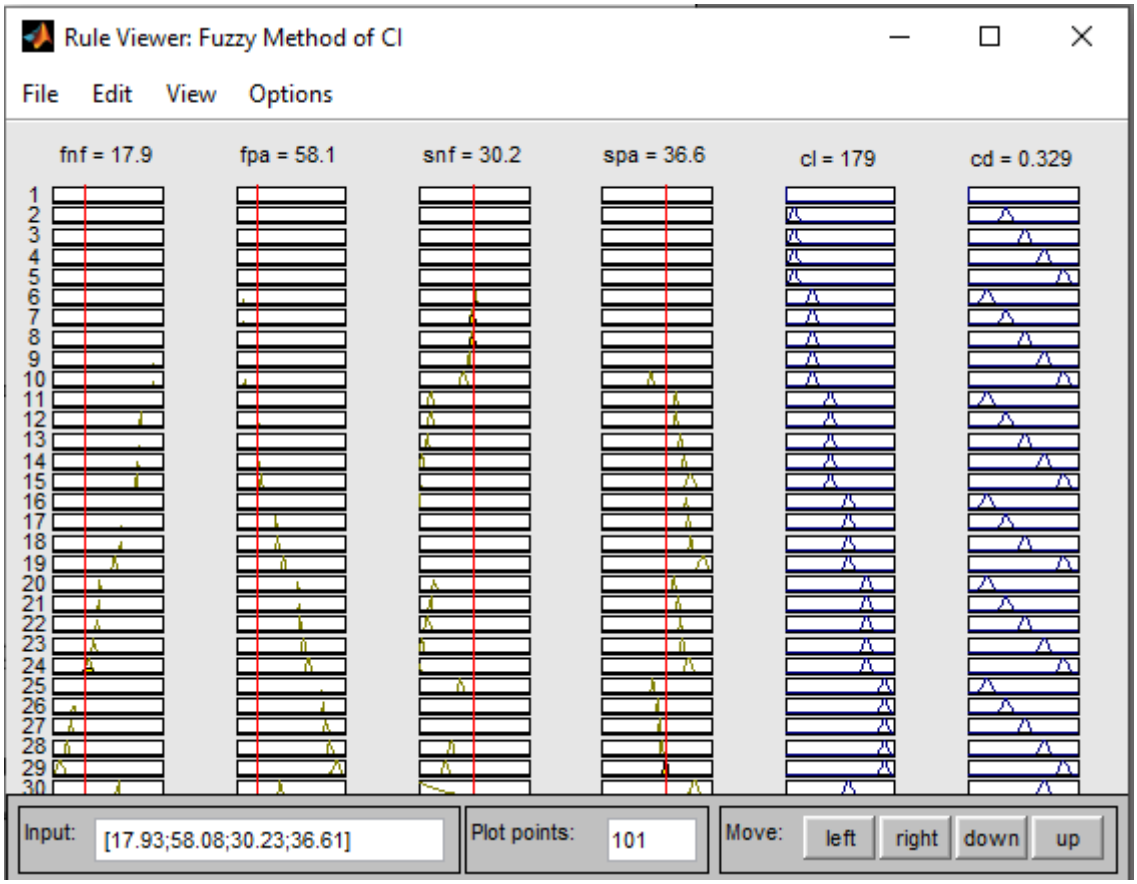

Figure 2: Fuzzy cluster analysis used for crack identification

Appendix B

Equations of Correlation coefficient and Average total error

1. **Correlation coefficient *r*;**

$$r = S_{XY} / \sqrt{S_{XX} S_{YY}}$$

where; S_{XX}, S_{YY}, *and* S_{XY} *are sum of the squares about the mean.*

$$S_{XX} = \sum w_i (x_i - \overline{x})^2$$

$$S_{YY} = \sum w_i (y_i - \overline{y})^2$$

$$S_{XY} = \sum w_i (x_i - \overline{x})(y_i - \overline{y})$$

where; w_i is the weight and the means of x and y are explained as follows;

$$\overline{x} = \sum w_i x_i / \sum w_i$$

$$\bar{y} = \sum w_i y_i / \sum w_i$$

2. **Average Total Error E_{AV};**

$$E_{AV} = \sum_{i=1}^{n} E_i / \sum n$$

$$where; E\ is\ the\ error = \left| \frac{Known\ value - Proposed\ value}{Known\ value} \right| * 100$$

and n is the number of samples

Appendix C

Correlation coefficient factor and average total error of different fuzzy controller membership functions with the theoretical location and crack depth ratio.

Table 1: Results from triangular membership functions

Theoretical crack location, crack depth ratio and Vibration parameters obtained from Matlab						Crack location and depth obtained from **triangular** MF	
cl	cdr	fnf	fpa	snf	spa	cl	cdr
89.4	0.2	18.0292	58.0303	30.2251	36.6136	89.93	0.1983
89.4	0.3	18.0289	58.0313	30.2251	36.6137	89.93	0.2984
149	0.3	18.0083	58.0867	30.2236	36.6154	149.9	0.2984
149	0.4	18.0068	58.0909	30.2234	36.6156	149.9	0.3983
208.6	0.4	17.9779	58.1691	30.2229	36.6161	209	0.3982
208.6	0.5	17.9733	58.1815	30.2226	36.6165	209	0.5079
268.2	0.2	17.9504	58.2436	30.2237	36.6153	268.5	0.1982
268.2	0.3	17.9479	58.2503	30.2236	36.6154	268.5	0.2984
327.8	0.4	17.9057	58.3651	30.2244	36.6145	327.9	0.3983
327.8	0.5	17.896	58.3916	30.2242	36.6147	327.9	0.5076
Correlation coefficient						**0.9993**	**0.9993**
Average total error (%)						**0.3058**	**0.7749**

Table 2: Results from trapezoidal membership functions

Theoretical crack location, crack depth ratio and Vibration parameters obtained from Matlab						Crack location and depth obtained from **trapezoidal** MF	
cl	cdr	fnf	fpa	snf	spa	cl	cdr
89.4	0.2	18.0292	58.0303	30.2251	36.6136	90.22	0.1237
89.4	0.3	18.0289	58.0313	30.2251	36.6137	90.22	0.2976
149	0.3	18.0083	58.0867	30.2236	36.6154	149.5	0.2976
149	0.4	18.0068	58.0909	30.2234	36.6156	149.5	0.3975
208.6	0.4	17.9779	58.1691	30.2229	36.6161	209.2	0.3975
208.6	0.5	17.9733	58.1815	30.2226	36.6165	209.2	0.5112
268.2	0.2	17.9504	58.2436	30.2237	36.6153	268.4	0.1974
268.2	0.3	17.9479	58.2503	30.2236	36.6154	268.4	0.2976
327.8	0.4	17.9057	58.3651	30.2244	36.6145	328	0.3975
327.8	0.5	17.896	58.3916	30.2242	36.6147	328	0.5112
Correlation coefficient						**0.9990**	**0.9878**
Average total error (%)						**0.3354**	**4.8205**

Table 3: Results from Gaussian membership functions

Theoretical crack location, crack depth ratio and Vibration parameters obtained from Matlab						Crack location and depth obtained from **Gaussian** MF	
cl	cdr	fnf	fpa	snf	spa	cl	cdr
89.4	0.2	18.0292	58.0303	30.2251	36.6136	90	0.2
89.4	0.3	18.0289	58.0313	30.2251	36.6137	90	0.3002
149	0.3	18.0083	58.0867	30.2236	36.6154	149.6	0.3003
149	0.4	18.0068	58.0909	30.2234	36.6156	149.6	0.4121
208.6	0.4	17.9779	58.1691	30.2229	36.6161	209	0.4028
208.6	0.5	17.9733	58.1815	30.2226	36.6165	209	0.5
268.2	0.2	17.9504	58.2436	30.2237	36.6153	268	0.2001
268.2	0.3	17.9479	58.2503	30.2236	36.6154	268	0.3003
327.8	0.4	17.9057	58.3651	30.2244	36.6145	328.2	0.407
327.8	0.5	17.896	58.3916	30.2242	36.6147	328.2	0.5
Correlation coefficient						**0.9998**	**0.9997**
Average total error (%)						**0.2926**	**0.5792**